LOCAL DEFORMATION OF THE ERYTHROCYTE MEMBRANE

LOCAL DEFORMATION OF THE ERYTHROCYTE MEMBRANE INDUCED BY FOCUSED LIGHT ILLUMINATION

By

FELIX HAU CHUN WONG, B.Sc.

A Thesis

Submitted to the School of Graduate Studies

in Partial Fulfillment of the Requirements

for the Degree

Master of Science

McMaster University

MASTER OF SCIENCE (2005) McMaster University

(Physics and Astronomy) Hamilton, Ontario, Canada

TITLE: Local Deformation of the Erythrocyte Membrane Induced by Focused Light Illumination

AUTHOR: Felix Hau Chun Wong, B.Sc. (McMaster University)

SUPERVISOR: Dr Cecile Fradin

NUMBER OF PAGES: xi, 58

Abstract:

A rapid local deformation of the erythrocyte membrane in the shape of an imprint caused by illumination with a focused laser beam in the presence of an external fluorophore has been investigated. This morphological change of the membrane appeared to be the very first observable step of the photohemolysis process which is exploited in photodynamic therapy. I showed that when a laser beam was focused on the erythrocyte membrane, the membrane was pulled toward the inside of the cell, independently of the direction in which the light was traveling. Imprint formation was observed neither on the lipid membrane of giant unilamellar vesicles nor on the membrane of nucleated mammalian cells such as HeLa cells. It shows that the effect is specific to erythrocytes; suggesting that it might be due to the unique structure of the erythrocyte membrane cytoskeleton. Also, I found that the rate of the imprint formation depended on laser input power, fluorophore concentration, and the presence of oxygen scavenger, but that it was independent of pH in the range pH = 6.4 to 7.8. These dependences are exactly the same for photohemolysis and for the imprint formation. By analogy with the photohemolysis process, these observations suggest that the imprint is created via the oxidization of band 3 proteins on the erythrocyte membrane. It supports the hypothesis that band 3 proteins play a pivotal role in the preservation of the erythrocyte shape. Preliminary work also suggests that spectrin is involved in the imprint formation process.

Acknowledgements

It is difficult to overstate my gratitude to my supervisor, Dr. Cecile Fradin, for her guidance and support throughout the course of my research, and all the helpful comments and ideas in this thesis. Her patience and good advices encourage me through the difficult time during my research.

I thank my committee members, Dr. Kari Dalnoki-Veress, Dr. Harold Haugen, and Dr. Tom Farrell, for all the comments and suggestions in the committee meetings.

I am indebted to many people for their help in my research. I thank Dmitri Satsoura for helping me to prepare the vesicle sample and Ajit Thakur and Asmahan Abu-Arish for preparing HeLa cell sample. I also thank Josh Ng for providing the confocal microscopy images of red blood cells. I own many thanks to Dr. Richard Epand and Dr. Raquel Epand for the explanations and the help on the Differential Scanning Calorimetry experiments. In addition, I thank Dr. Brian Leber for providing the blood sample for the Differential Scanning Calorimetry experiments.

I also thank Daniel Banks for the helpful editing suggestions in this thesis.

I am grateful to the members in Fradin's group for providing a stimulating and fun environment to work and learn.

At last, and most importantly, I thank my parents and my brother for their supports and loves.

Table of Contents

	Page
Descriptive Note	ii
Abstract	iii
Acknowledgements	iv
Table of Contents	v
List of Figures	viii
List of Table	xi
Chapter 1 Background	1
1.1 Erythrocyte	1
1.1.1 Hemoglobin	2
1.1.2 Membrane cytoskeleton	3
1.1.2.a General structure	3
1.1.2.b Spectrin	4
1.1.2.c Band 3	5
1.2 Erythrocyte elasticity and shape	7
1.2.1 Membrane elasticity	7
1.2.2 Bilayer coupled hypothesis	8
1.2.3 Band 3 conformation-controlled bilayer couple model	9
1.2.4 Area difference elasticity model of shape calculation	10
1.2.5 Band 3 protein conformation model	11
1.3 Photosensitization	12
1.3.1 Photosensitization by type I and type II mechanisms	13
1.3.2 Photosensitization on erythrocytes	14

Chapter 2 Materials and Methods 16

2.1 Sample Preparations 16

2.1.1 Preparation of erythrocytes 16

2.1.2 Preparation of resealed erythrocyte ghosts 16

2.2 Experimental setup 17

2.3 Determination of the erythrocyte membrane position 19

2.4 Autocorrelation function analysis 21

2.5 Calibration 21

2.6 Membrane kinetics experiments 22

Chapter 3 Results 24

3.1 Photodamage induced by focused laser beam illumination 24

3.2 Control experiments 25

3.3 Intensity trace recorded during photohemolysis 27

3.4 Imprint characterization 28

3.4.1 Direction of the membrane shift 28

3.4.2 Membrane integrity 30

3.4.3 Reversibility of imprint formation 31

3.4.4 Investigation of imprint formation on the rim and on the dimple of the erythrocytes 33

3.4.5 Formation of two imprints on the same erythrocyte 34

3.5 Kinetics of photohemolysis and imprint formation 35

3.5.1 Dependence on fluorophore concentration 35

3.5.2 Dependence on laser input power 36

3.5.3 Effect of pH 37

3.5.4 Overall rate equations 37

3.6 Investigation of the influence of protecting substrates against photodamage 38

3.7 Focused laser beam illumination on GUVs and HeLa cells 39

3.8 Role of erythrocyte components on imprint formation 41

3.8.1 Imprint formation on erythrocyte ghost 41

3.8.2 Imprint formation on spherical erythrocyte after thermal treatment 41

Chapter 4 Discussions 43

4.1 What is the cause of the imprint? 43

4.2 What is the primary target of the photodamage on the erythrocyte? 45

4.3 Photodamage kinetics of focused and wide-field illumination 46

4.4 Localized vs long range photodamage on the erythrocyte membrane 47

4.5 Models of erythrocyte shape transformation 48

4.6 Involvement of spectrin in imprint formation 49

Chapter 5 Conclusions 52

References 53

LIST OF FIGURES

Page

Chapter 1 Background

Figure 1. Scanning electron microscope images of erythrocytes in various morphologies 2

Figure 2. A model of the erythrocyte membrane skeleton with its major components 4

Figure 3. Electron micrographs of the erythrocyte spectrin network 5

Figure 4. Schematic representation of the bilayer coupled theory of cell shape changes 9

Figure 5. Schematic diagram of the band 3 transmembrane domain proposed by Gimsa and Ried 10

Figure 6. Minimum energy shapes calculation using area difference elasticity model of normal biconcave erythrocyte, echinocyte, and stomatocyte 11

Figure 7. A schematic diagram of the mechanism proposed for erythrocyte shape transformation by P. Wong 12

Chapter 2 Materials and Methods

Figure 8. Schematic diagram of the experimental setup including an example of a recorded one dimensional intensity profile 17

Figure 9. Front panel of the modified experiment control program written using LabView 19

Figure 10. Intensity trace recorded during the erythrocyte membrane local deformation induced by illumination of the erythrocyte membrane 23

Chapter 3 Results

Figure 11. DIC images and schematic representations of RBC photohemolysis at different stages 24

Figure 12. The correlation between the time spent by the erythrocytes in vitro and the hemolysis time 25
Figure 13. Hemolysis time obtained for various vertical position of the laser focus 26
Figure 14. Fluorescence intensity trace recorded during the hemolysis induced by focused laser beam illumination 27
Figure 15. Intensity profiles recorded along a vertical axis of an erythrocyte's rim region when the cell was attached on the bottom glass in the sample chamber 29
Figure 16. Intensity profile recorded along a vertical axis of an erythrocyte's rim region when the cell was attached on the top glass in the sample chamber 29
Figure 17. Intensity traces recorded on the erythrocyte lower membrane 30
Figure 18. DIC and wide-field fluorescence images of erythrocytes before and after the imprint formation 31
Figure 19. Intensity trace recorded on an erythrocyte membrane with a sequence of switching on and off the laser illumination 32
Figure 20. Intensities recorded before and after the off period of the laser illumination from samples with different combinations of on and off period time 32
Figure 21. Intensity trace recorded at the rim region and at the dimple for two different erythrocytes 33
Figure 22. Intensity trace of two imprints formation on the same cell 34
Figure 23. Average hemolysis time and time constant of imprint formation recorded for various fluorophore concentrations. Average change in membrane position during the imprint formation recorded for various fluorophore concentrations. 35
Figure 24. Average hemolysis time and time constant of imprint formation recorded for various laser input powers. Average change in membrane position during the imprint formation recorded for various laser input powers. 36

Figure 25. Average time constant of imprint formation recorded for a pH range of 6.4 to 7.8 37
Figure 26. Relative intensity trace recorded on two GUVs and an erythrocyte 40
Figure 27. Relative intensity trace recorded on a HeLa cell and an erythrocyte 40
Figure 28. DIC images of a resealed erythrocyte ghost before laser illumination and after laser illumination 41
Figure 29. DIC images of a spherical erythrocyte after a 49°C temperature treatment for 10 min 42

Chapter 4 Discussions

Figure 30. Confocal microscope images of RBCs immunolabeled with an antibody against band 3 with and without wide-field illumination before immunolabeling 46
Figure 31. DSC scans (40-75°C) of human erythrocyte ghost with and without hemoglobin. 51

LIST OF TABLES

Page

Chapter 3 Results

Table 1: Values of total time constants and time constants with off period removed for different on and off illumination periods 33

Chapter 1 Background

1.1 Erythrocyte

Erythrocytes, commonly known as red blood cells, are important to many animals. The main function of the erythrocyte is to transport oxygen and carbon dioxide when it circulates the body. Erythrocyte concentration in human blood is around 5 billion cells per liter. Erythrocytes are generated in the bone marrow, and they have a life span of 120 days on average. The spleen filters the old and damaged erythrocytes. Erythrocytes contain no internal membrane, nucleus, or internal organelles; therefore, the erythrocyte membrane becomes an ideal model for more complex cell membranes. A highly concentrated hemoglobin solution fills the cytoplasm; thus, an erythrocyte can be thought of as a membranous bag of hemoglobin. A normal erythrocyte, also called a discocyte, has a biconcave disc shape with a rim and a dimple region. The mean diameter of a discocyte is 7.65 μm. The rim region has a mean thickness of 2.84 μm, and the mean thickness of the dimple region is 1.44 μm. The surface area and volume of an erythrocyte are 129.95 μm^2 and 97.91 μm^3 respectively (Fung, Tsang et al. 1981). Other cell morphologies, echinocytes (spiculated spherical shapes) and stomatocytes (cup-like shapes), can be observed when the cells are exposed to various conditions (Fig. 1), such as variation of pH (Gedde, Yang et al. 1995; Gedde, Yang et al. 1999) or ATP level in the cell (Nakao, Nakao et al. 1961; Nakao 2002).

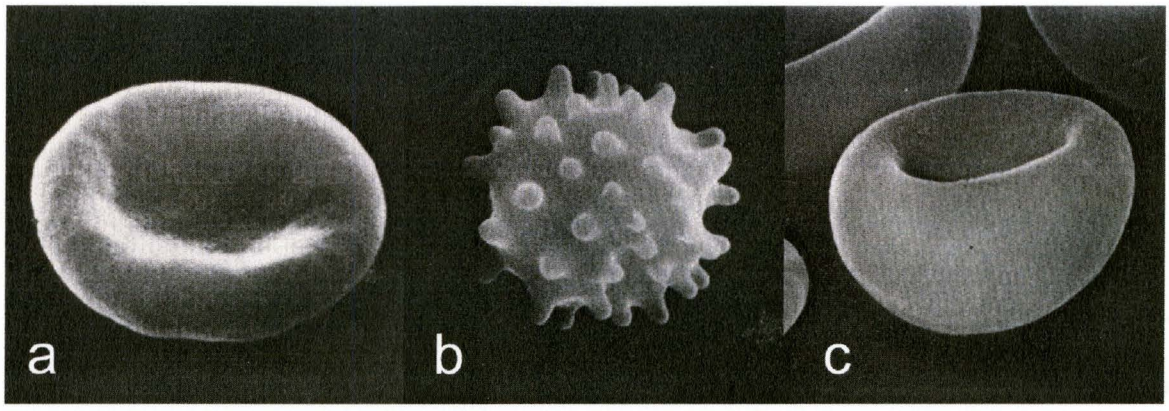

Figure 1. Scanning electron microscope images of erythrocytes in various morphologies. a) Normal erythrocyte. b) Echinocyte. c) Stomatocyte (Bessis 1973).

1.1.1 Hemoglobin

Hemoglobin is the intracellular protein that gives the erythrocyte its red color, and it is the major light-absorbing component within the cell. The function of hemoglobin is to carry oxygen or carbon dioxide. Hemoglobin is a tetrameric protein formed of two alpha and two beta subunits (Voet, Voet et al. 1999). Each subunit is made of a heme imbedded in a globular protein. The binding of oxygen to the hemoglobin is a cooperative process. When oxygen binds to one subunit, this increases the affinity of oxygen for the other subunits. The cooperativity goes the same way for unbinding of the oxygen. When a bicarbonate ion (which is the dissolved form of carbon dioxide) binds to hemoglobin, a conformational change of the hemoglobin occurs. The result is the release of oxygen from the hemoglobin. Mutations of the hemoglobin gene can result in diseases such as sickle-cell anemia (Bertles and Milner 1968).

1.1.2 Membrane cytoskeleton

1.1.2.a General structure

The primary function of the red blood cell membrane is to serve as a boundary between the cell cytoplasm and the surrounding medium. Since the erythrocytes lack internal cell organelles, their membranes are also responsible for maintaining their distinctive morphology. During blood circulation, erythrocytes are squeezed through small capillaries repeatedly without permanent cell shape distortion. A unique cell membrane structure provides this extraordinary cell elasticity and gives erythrocytes their ability to change shape. The red blood cell membrane is made of a phospholipid bilayer. Beneath the lipid bilayer, there is a protein network forming the cell cytoskeleton (Fig. 2). Many membrane proteins of the erythrocyte membrane are named according to a band index system due to their early analysis by gel electrophoresis (Fairbanks, Steck et al. 1971). The main component of the cytoskeleton is a long flexible protein called spectrin. Spectrin molecules are assembled in tetramers which form a network connected to the lipid bilayer through two different transmembrane proteins, band 3 and glycophorin C. The first anchoring sites are near the mid-region of the spectrin tetramers. At these sites, the spectrin connects to band 3 through ankyrin (Bennett and Stenbuck 1979; Tyler, Hargreaves et al. 1979) with the association of band 4.1 and band 4.2 (Korsgren and Cohen 1986). The second sites are at the actin-spectrin junctional complexes that connect spectrin tetramers together through short actin filaments (Ungewickell, Bennett et al. 1979; Byers and Branton 1985). Glycophorin C bind to spectrins via band 4.1 on the junctional complexes at the end of the spectrins (Tyler, Hargreaves et al. 1979; Anderson and Lovrien 1984). The bindings of the spectrins and the short actin filaments are enhanced by band 4.1 (Ohanian, Wolfe et al. 1984). Each complex also associates with other proteins such as p55 (Alloisio, Dalla Venezia et al. 1993) and adducin (Gardner and Bennett 1987). In addition, erythrocytes contain membrane cytoskeleton components such as tropomyosin, tropomoduluin, and capZ, and mobile proteins on the cell surface

such as aquaporin and GPI-linked proteins (reviewed in (Bennett and Baines 2001; Discher and Carl 2001)).

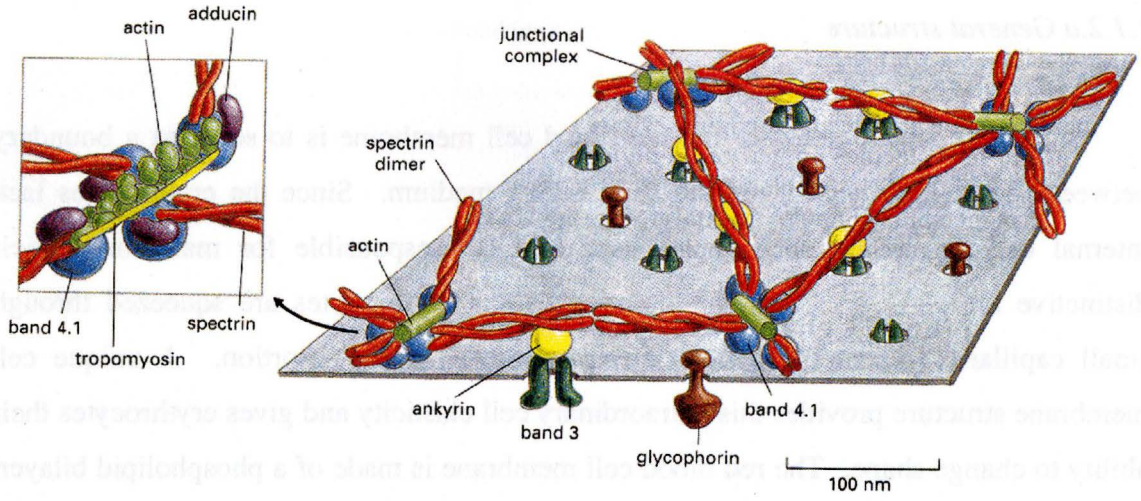

Figure 2. A model of the erythrocyte membrane skeleton with its major components (Alberts, Bray et al. 1994).

1.1.2.b Spectrin

Spectrin is the major component of the erythrocyte cytoskeleton. There are two subunits of spectrin found in erythrocytes, band 1 (α subunit) and band 2 (β subunit), and their molecular weights are estimated to be 280kD (Sahr, Laurila et al. 1990) and 246kD (Winkelmann, Chang et al. 1990) respectively by their cDNA sequences. Each subunit is a flexible rod in solution of around 100nm in length. The two subunits are loosely coiled around each other forming a flexible heterodimer (Shotton, Burke et al. 1979). Two heterodimers then associate together to form a tetramer in a head-to-head manner (Liu and Palek 1980). In each erythrocyte, there are roughly 250,000 spectrin tetramers. Each tail-end can bind to two or three spectrin tetramers at a junctional complex to form a dense protein meshwork underneath the plasma membrane. The role of spectrin in the erythrocyte cytoskeleton is demonstrated in the case of diseases caused by spectrin deficiency such as hereditary elliptocytosis, in which the shape of erythrocytes changes to elliptocytic. Spectrin deficiency can also lead to hemolytic anemia in patients because of

poor cell shape changing capability during blood circulation (reviewed in (Liu and Derick 1992)). This shows that spectrin is essential for both maintaining cell shape and cell elasticity.

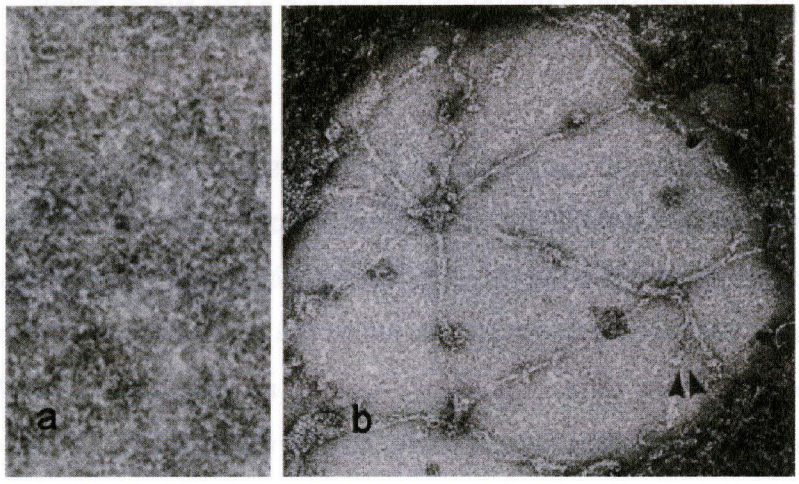

Figure 3. Electron micrographs of the erythrocyte spectrin network. a) Intact erythrocyte spectrin network (145,500x magnification). b) Spread erythrocyte spectrin network (200,000x magnification). Between four and seven spectrin molecules connect together through the junctional complexes and form the membrane skeleton (Byers and Branton 1985).

1.1.2.c Band 3

Band 3 is an integral membrane protein and there are about 1.2 million copies of band 3 on the erythrocyte plasma membrane, which represents roughly 25% of the total membrane skeleton proteins, and a density of roughly 8500 copies of band 3 per μm^2 (Lepke, Fasold et al. 1976). Band 3, sometimes called anion exchanger I (AE1), serves as an anion transport protein on the erythrocyte membrane, playing an important role in carbon dioxide transport. Carbon dioxide is carried in the blood as bicarbonate anion due to the low solubility of carbon dioxide. The bicarbonate anion is transported in and out of the erythrocyte in exchange for a chloride anion through the band 3 protein (reviewed in (Wang 1994)). Band 3 proteins also act as senescent cell antigens on damaged or old erythrocytes, forming integral membrane clusters which stimulate the binding of antibodies and removal of the erythrocytes from the blood plasma (Turrini, Arese et al.

1991). In addition, band 3 proteins are essential in erythrocyte morphology. Band 3 mutation in hereditary spherocytosis and Southeast Asian ovalocytosis also shows the role of band 3 in cell morphology and cell rigidity (reviewed in (Kay 2004)). Furthermore, most of the band 3 inhibitors can induce a cell shape change from discocyte to echinocyte.

Band 3 proteins exist as a mixture of dimers and tetramers in the erythrocyte membrane (reviewed in (Low 1986)). Each band 3 protein contains two distinct domains, the transmembrane domain and the cytoplasmic domain. The transmembrane domain is a 55kD fragment at the carboxyl-terminal. It spans the plasma membrane multiple times. The main function of this domain is to provide the anion transport capability. It also contains the binding site of the senescent cell antigens (Kay 1984). The second domain is the cytoplasmic domain, a 42kD fragment at the amino-terminal. The cytoplasmic domain of band 3 provides binding sites for the membrane cytoskeleton proteins, spectrin, ankyrin, and band 4.1. It is probably through these associations that band 3 plays a role in the cell morphology and the mechanical strength of the cell. The extreme end of the cytoplasmic domain provides binding sites for glycolytic enzymes, hemoglobin, and hemichromes (reviewed in (Low 1986)). Proteolytic enzyme removal of the cytoplasmic domain apparently has no influence on the anion transport function of the transmembrane domain (Lepke and Passow 1976). Also, the two domains of band 3 proteins rotate independent of each other (Beth, Balasubramanian et al. 1981; Cassoly 1982). The above observations show that there is minimal interaction between the cytoplasmic domain and the transmembrane domain; hence, it suggests that there is a flexible hinge-like region either in the cytoplasmic domain (Low 1986) or between the two domains (Wang 1994). The recent lateral diffusion of band 3 study at 37°C using single particle tracking by Tomishige and colleagues reveals that one-third of the band 3 exhibit oscillatory motion only, and the rest of the band 3 diffuses across the membrane surface with hopping diffusion mechanism (Tomishige, Sako et al. 1998). The oscillatory motion is due to the binding of band 3 to the spectrin network. On the other hand, the free band 3 diffuses in a

confined corral and then hops to an adjacent corral every 350 ms. It is suspected that the confinement of band 3 is due to the cytoplasmic domain of the band 3 extending beyond the plane of the spectrin network; therefore, it diffuses in the corral and collides with the membrane skeleton. In support of this hypothesis, the authors have shown that when the cytoplasmic domain of the band 3 is removed, the hopping rate increases 6-fold.

1.2 Erythrocyte elasticity and shape

1.2.1 Membrane elasticity

An understanding of erythrocyte elasticity and its mechanism of shape change should rely on the elastic properties of the membrane and the associated cytoskeleton itself because of the lack of internal organelles in erythrocytes. For small deformations, the membrane response to a given stress is characterized by three elastic moduli: bending rigidity, shear modulus, and compression (or stretch) modulus. These moduli have been studied intensively using different techniques, and the measured parameters are routinely used to model the erythrocyte. The bending rigidity, κ, is the elastic constant that indicates the resistance of a membrane to curvature change (Boal 2002). For red blood cells, a recent atomic force microscope experiment found $\kappa = 50\ k_BT$ (Scheffer, Bitler et al. 2001), higher than the value $\kappa = 3\text{-}8\ k_BT$ measured roughly thirty years ago (reviewed in (Boal 2002)). The shear modulus, μ, is the elastic constant which characterizes the response of the membrane cytoskeleton to shear stress (Boal 2002). A recent micropipette aspiration experiment showed that $\mu = 2.4\ \mu N/m$ in hypotonic buffer and $\mu = 7.9\ \mu N/m$ in isotonic buffer (Lenormand, Henon et al. 2001). Meanwhile, an optical tweezers experiment gave $\mu = 2.5\ \mu N/m$ (Henon, Lenormand et al. 1999). The compression modulus is another elastic constant which represents the magnitude of the change in area in response to lateral pressure exerted on the membrane (Boal 2002). Micropipette aspiration experiments revealed an area compression modulus $K = 4.8\ \mu N/m$

(roughly two times the shear modulus) in hypotonic buffer and K = 22.6 μN/m (roughly three times the shear modulus) in isotonic buffer (Lenormand, Henon et al. 2001). The erythrocyte membrane resistance to bending is thought to come from the lipid bilayer, while the membrane resistance to shear and stretch is thought to come from the cytoskeleton.

1.2.2 Bilayer coupled hypothesis

Sheetz and Singer proposed that the two lipid layers of the closed surface membrane of the erythrocyte can act as bilayer couples with proteins and polar lipids distributed asymmetrically in the two membrane leaflets. The erythrocyte morphological transformation is the result of the change in the difference in surface area between the two leaflets of the plasma membrane (Sheetz and Singer 1974; Sheetz, Painter et al. 1976). When the area of the membrane outer leaflet increases, the erythrocyte transforms from discocyte to echinocyte. In contrast, the cell transforms from discocyte to stomatocyte when the surface area of the inner leaflet increases. This simple theory can explain cell morphological change when more phospholipids (Christiansson, Kuypers et al. 1985) and cholesterols (Lange and Slayton 1982) insert into different leaflets. Experiments showed that discocytes turn into echinocytes after inserting additional phospholipids or cholesterols into the outer leaflets. In contrast, discocytes turn into stomatocytes when phospholipids are inserted into the inner leaflets. Also changes in area difference can happen if phospholipids or cholesterols flip from one leaflet to the other; again, creating shape transformation. All in all, the bilayer coupled theory can explain most of the erythrocyte morphological transformations, although not all. For example, erythrocyte shape can be varied with the external pH; high pH promotes echinocyte and low pH promotes stomatocyte. Unfortunately, this observation is hard to fit in with the bilayer coupled hypothesis alone, so that other effects probably also play a role.

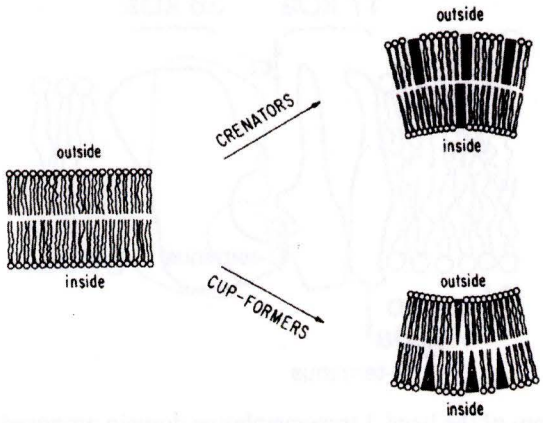

Figure 4. Schematic representation of the bilayer coupled theory of cell shape changes. The area difference of the two membrane leaflets is due to the insertion of lipids or cholesterols into either leaflet (Sheetz and Singer 1974).

1.2.3 Band 3 conformation-controlled bilayer couple model

Gimsa and Ried proposed a mechanism of erythrocyte shape changes that combines the bilayer coupled hypothesis with band 3 protein conformational changes (Gimsa and Ried 1995). Passow suggested that anions are transported across the erythrocyte membrane by a ping pong mechanism, where band 3 alternates between two conformations during anion transport, each of them exposing the transport site on a different side of the membrane (Passow 1986). Gimsa and Ried assume that the transport site can slightly increase the surface area of the leaflet that it faces. They also assume that various physiological conditions alters the ratio of the outward to inward facing anion transport sites of the transmembrane domain of band 3 on the erythrocyte membrane. Since there are around 1.2 million copies of band 3 per erythrocyte, all band 3 proteins taking the same conformation should alter the total area difference between the two membrane leaflets significantly. The change in relative surface area of the two membrane leaflets results in erythrocyte shape transformations to echinocyte or stomatocyte as explained by the bilayer coupled theory.

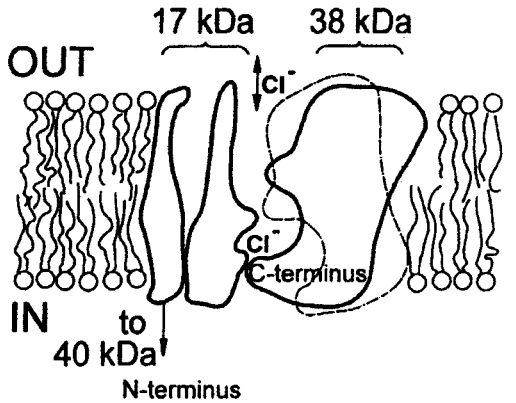

Figure 5. Schematic diagram of the band 3 transmembrane domain proposed by Gimsa and Ried. The 38kDa protein segment drawn with a solid line indicates the outward facing conformation of band 3 which slightly increases the surface area of the outer leaflet. The 38kDa segment drawn with dotted line indicates the inward facing conformation of band 3 which slightly increases the surface area of the inner leaflet (Gimsa and Ried 1995).

1.2.4 Area difference elasticity model and shape calculation

Continuum mechanics can be combined with bilayer coupled theory in order to characterize the erythrocyte morphology and morphological transformations by a mathematical approach. Waugh, Iglič and colleagues (Iglic 1997; Iglic, Kralj-Iglic et al. 1998), and Mukhopadhyay and colleagues (Mukhopadhyay, Lim et al. 2002) were able to predict the echinocyte shape using such an area difference elasticity model. The erythrocyte shape is determined by the minimization of the membrane elastic energy with the appropriate constraints. The membrane surface area and the cell volume are fixed in the calculation. Also, the model depend on the choice of an equilibrium shape for the cytoskeleton. The membrane elastic energy includes the local and non-local bending energy of the lipid bilayer, and the shear and stretch energy of the membrane cytoskeleton. The bilayer local bending energy is the energy density related to the bending rigidity and the two local principle curvatures integrated over the whole surface area of the cell. The non-local bending energy is the bending resistance of the bilayers related to the area difference of the two leaflets. The cytoskeleton shear energy is the energy density related to the shear modulus and the shear deformation of the membrane skeleton. The

cytoskeleton stretch energy is the energy related to the area stretching modulus and the change in cytoskeleton network surface area. Mukhopadhyay and colleagues calculate the minimum-energy shapes by fixing most of the parameters in this model except the area difference between the outer leaflet and the inner leaflet, ΔA_0 (Lim, Wortis et al. 2002). Consequently, they can calculate various erythrocyte shapes by varying ΔA_0 only. Furthermore, they find that increasing ΔA_0 promotes cell shape to echinocyte, and decreasing ΔA_0 promotes cell shape to stomatocyte. The shape transformation with the change in ΔA_0 in this model agrees with the bilayer coupled theory.

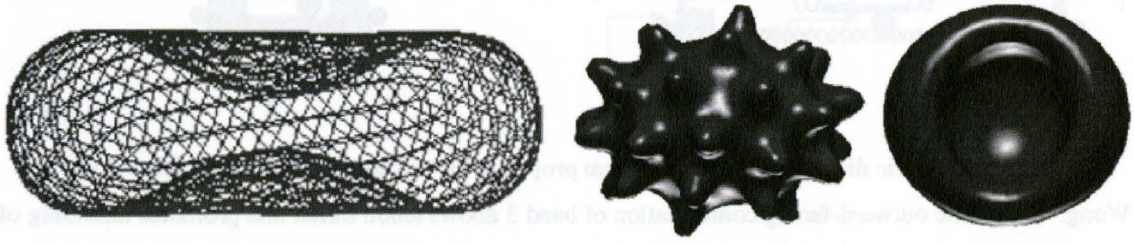

Figure 6. Minimum energy shapes calculation using area difference elasticity model of normal biconcave erythrocyte, echinocyte, and stomatocyte (from left to right) (Lim, Wortis et al. 2002).

1.2.5 Band 3 protein conformation controlled folding of spectrin model

Wong proposed a theoretical model for the erythrocyte morphological transformation as a result of the conformational change of band 3 proteins (Wong 1994; Wong 1999). This model, like the model proposed by Gimsa and Ried, assumes that there are two different conformations of band 3 proteins, outward-facing and inward-facing (reviewed in (Knauf, Gasbjerg et al. 1996)). This model further assumes that a conformational change of the transmembrane domain of band 3 is accompanied by a conformational change of the cytoplasmic domain of band 3, and that this reaction either folds or unfolds the spectrin. The fraction of folded spectrin is then determined by the ratio of outward-facing to inward-facing band 3. An increase in chloride ions outside the cell promotes the anion influx, which increases the number of outward-facing band 3; hence, this increases the fraction of unfolded spectrins according to the model. Unfolding of spectrin promotes the relaxation of the erythrocyte cytoskeleton, and a cell shape

change to stomatocyte. An anion efflux, on the other hand, increases the number of inward-facing band 3, which increases the fraction of the folded spectrins. Echinocyte shapes are then promoted due to the contraction of the cytoskeleton. This is the only model giving a crucial role to the cytoskeleton. Unfortunately, this model so far lacks direct support from experimental evidence. It also does not clarify how extension of the spectrin network leads to shape change.

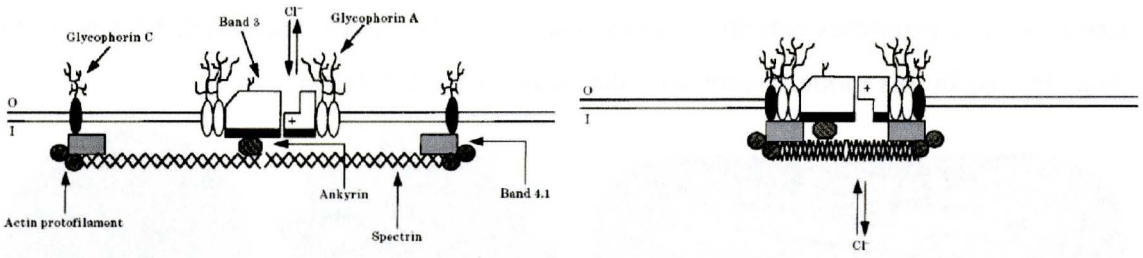

Figure 7. A schematic diagram of the mechanism proposed for erythrocyte shape transformation by P. Wong. (Left) The outward-facing conformation of band 3 allows anion influx and promotes unfolding of spectrin. (Right) The inward-facing conformation of band 3 allows anion efflux and promotes folding of spectrin (Wong 1999).

1.3 Photosensitization

When a photosensitizer, or fluorophore, absorbs a photon with enough energy, it excites the photosensitizer from a ground state to its first higher energy electronic state. The sensitizer has a short life time in this excited state (~ 1 – 100 ns) (Spikes 1989). Emission of light in the form of fluorescence is a direct method for the sensitizer to decay to the ground state. Although fluorescence usually refers to singlet to singlet transition, the sensitizer can also be excited to second or higher excited states and decay to the first excited state through internal conversion. Afterward, the sensitizer decays to the ground state via fluorescence. On the other hand, the sensitizer in the singlet excited state can undergo an intersystem crossing to a triplet excited state. This occurs through a spin inversion of the excited electron resulting in the two unpaired electrons of the molecule having the same spin orientation. Sensitizers in the triplet excited state have a rather long life time, ranging from microseconds to seconds, and this allows the excited sensitizers to

undergo a large numbers of collisions with other molecules while in an excited state. The result of these collisions can be photosensitized reactions, where the triplet sensitizers return to their ground state by transferring energy to another substrate in the system. There are two types of mechanisms in photosensitization, type I and type II reactions (Spikes 1989).

1.3.1 Photosensitization by type I and type II mechanisms

A type I reaction refers to an electron transfer process (Spikes 1989). The triplet sensitizer can absorb and donate electrons more readily than in the ground state. This process creates free radicals after the triplet sensitizers have reacted with substrates in the system. The highly reactive free radicals can then react with biomolecules such as proteins and nucleic acids. A type II photosensitized reaction is an energy transfer process with oxygen (Spikes 1989). A triplet sensitizer can interact with a ground state oxygen molecule, which has a triplet ground state, and excite the oxygen molecule to an excited singlet state with high reactivity. Since most of the organic molecules are in the singlet ground state, the reaction of the singlet oxygen with these organic molecules is not spin forbidden. As a result, singlet oxygen can oxidize biomolecules effectively.

Both mechanisms can induce photooxidation that changes or destroys the normal biological function of a biomolecule. Photooxidation can induce the crosslinking of membrane proteins (Lepock, Thompson et al. 1978; Sheetz and Koppel 1979) and crosslinking between the two strands of double stranded DNA (Cadet, Berger et al. 1986). Photodynamic therapy (PDT) uses these mechanisms effectively in order to kill tumor cells (Hopper 2000). However, non-specific damage or destruction of healthy cells surrounding the tumor, especially erythrocytes, is a problem in PDT (Fischer, Aulmann et al. 1998).

1.3.2 Photosensitization on erythrocytes

Hemolysis is the breakdown of the erythrocyte membrane followed by the release of hemoglobin as an indicator. Studies of hemolysis induced by non-focused light illumination in presence of fluorophores are numerous. Early studies showed that exposure to light causes erythrocyte membrane protein cross-linking (Lepock, Thompson et al. 1978; Sheetz and Koppel 1979). Valenzeno and Pooler showed that the photohemolytic rate varies with both sensitizer concentration and light dose fluence, and follows a simple rate equation. Later, Pooler and Girotti found that hemolysis is more efficient when band 3 proteins on the erythrocyte membrane are labeled with photosensitizers before laser irradiation (Pooler 1986; Pooler and Girotti 1986). They proposed that photodamage of band 3 is the principal cause leading to photohemolysis (Pooler 1986). Damage of band 3 has also been linked to potassium leakage and indirectly linked to glucose leakage, both events being related to photohemolysis (Trannoy, Brand et al. 2002). Furthermore, band 3 proteins change conformation upon irradiation (Sato, Kamo et al. 1995), and the addition of an anion transport inhibitor, which binds to and stops the function of band 3, can reduce the photohemolytic rate (vanSteveninck, Trannoy et al. 2000; Trannoy, Brand et al. 2002). Band 3 photodamage is consequently the most likely candidate for the cause of photohemolysis. However other effects have been proposed: disorganization of the cellular membrane structure (Makropoulou, Serafetinides et al. 1995) and lipid peroxidation (Sato, Kamo et al. 1995) can also lead to photohemolysis.

On the other hand, only a handful of studies reported hemolysis induced by focused light illumination. When Ashkin and colleagues investigated the effect of cell trapping after inventing the optical tweezers, they observed laser light induced photodamage on cells (Ashkin and Dziedzic 1987; Ashkin, Dziedzic et al. 1987; Ashkin 1997; Ashkin 2000). They observed the immediate explosion of red blood cells and green cells containing chlorophyll after a 514.5nm HeNe laser with a power of 10mW

was focused on the cells (Ashkin 2000). They also found that cell damage is reduced when a near-infrared laser is using for the trapping (Ashkin, Dziedzic et al. 1987; Ashkin 1997; Ashkin 2000). Bloom and Webb investigated the photodamage of erythrocytes after exposure to a focused laser beam in fluorescence photobleaching recovery experiments that is in presence of exogenous fluorophores. In their description of the erythrocyte photodamage, they observed that there is always "a visible blemish or pucker" that forms on the cell membrane at the point illuminated by the laser before the erythrocyte changes morphology prior to hemolysis (Bloom and Webb 1984). They showed that the hemolytic rate depends on laser intensity and that there is a change in the dependence of the hemolysis time on laser intensity near 1mW. They proposed a calculation showing that the localized cell heating for a 1mW laser beam at 568nm focused to a 700nm radius is roughly 5°C, which is enough to give a thermal shock to the erythrocytes. In other words, thermolysis of the erythrocytes is dominant when the laser intensity is higher than 1mW (for λ = 568 nm), while photolysis is dominant for laser intensities below 1mW. In addition, they showed that the hemolytic rate depends on laser wavelength, fluorophore concentration, and that the presence of photodamage protecting substrates, and sample deoxygenation decreases the photohemolytic rate (Bloom and Webb 1984).

Chapter 2 Materials and Methods

2.1 Sample Preparations

2.1.1 Preparation of erythrocytes

The buffer mostly used for the erythrocytes (PBS-RBC buffer) was an isotonic PBS buffer (purchased from Bioshop, pH = 7.4) supplemented with 10 mM glucose and 1 mg/ml bovine serum albumin (BSA) (Tuvia, Levin et al. 1998). Fresh human blood was collected from an apparently healthy donor before every experiment, and 200μl of PBS-RBC buffer was added to 4μl of blood. The sample was centrifuged at 1500rpm for 2 min at 20°C. The supernatant was discarded after the centrifugation, and the erythrocyte pellet was resuspended in 200μl of PBS-BSA buffer. This washing step was repeated three times to remove all platelets and white blood cells from the blood sample and this also removed the serum proteins adhering on the erythrocyte membrane. After the last washing step, the erythrocyte pellet was resuspended in 800μl of PBS-RBC buffer to obtain a 0.5% hematocrit (erythrocyte concentration compared to its concentration in human blood). When necessary, either BSA conjugated with Alexa Fluor 488 (purchased from Molecular Probes, kept in a 10mg/ml stock solution in PBS at -20°C) or fluorescein (purchased from Sigma, kept in a saturated solution in PBS at room temperature) was diluted to an appropriate working concentration in the PBS-RBC buffer or directly in the erythrocyte sample. A fluorescein sample was also used to calibrate the size of the confocal detection volume. In this case, fluorescein was diluted in PBS to a final concentration of 50 to 80 nM.

2.1.2 Preparation of resealed erythrocyte ghosts

Erythrocytes ghosts are erythrocyte membranes from which hemoglobin has been removed by using osmotic lysis. Resealed erythrocyte ghosts have the same biconcave

shape as intact erythrocytes. The protocol used for the preparation of the resealed erythrocyte ghosts is a slightly modified version of the method described in Lee et al. (Lee, Wong et al. 1999). MgATP was added to the isotonic PBS buffer to obtain a final MgATP concentration of 5.5mg/mL. This solution was then diluted 10 times with deionized distilled water to prepare the RBC lysing buffer. The RBC lysing buffer (180µl) was added to the erythrocyte pellet after the washing steps described in the previous section to perform a hypotonic lysis. The sample was then incubated on ice for 4 minutes. Afterward, 20µl of a 10 times concentrated PBS solution was added to the sample, which was then incubated at 37°C for 1 hour. This step allows the membrane of the ghosts to reseal. The sample was then diluted in PBS-RBC buffer to a suitable working hematocrit.

2.2 Experimental setup

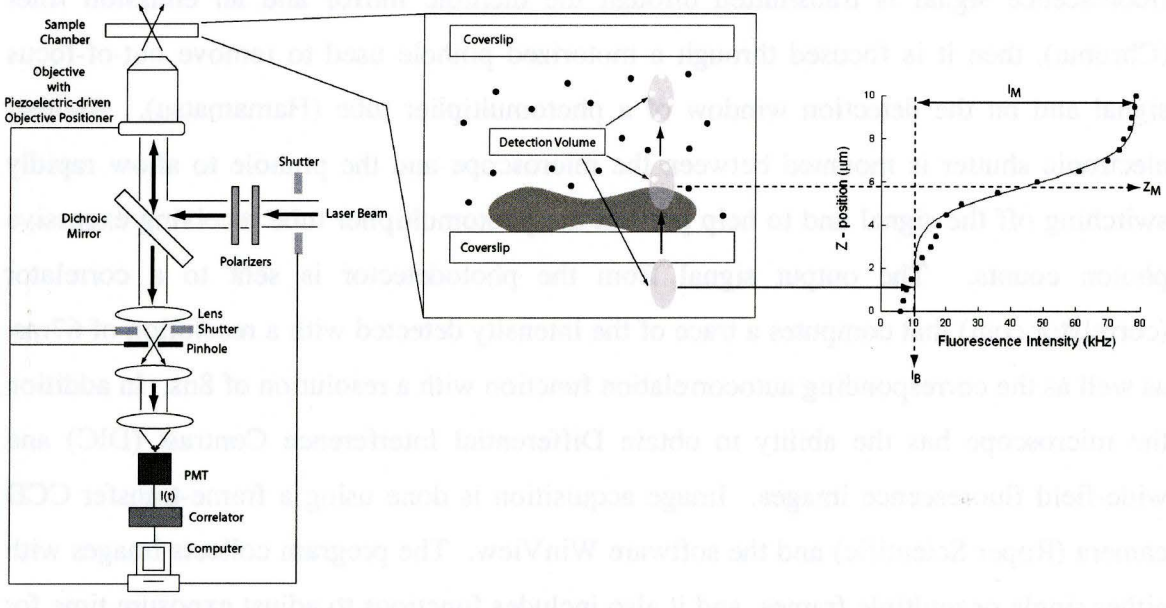

Figure 8. Schematic diagram of the experimental setup including an example of a recorded one dimensional intensity profile.

The schematic diagram of the experiment is shown in Fig. 8. The 488 nm emission of an argon-ion laser (Melles Griot) is attenuated by two polarizers to adjust the excitation intensity. The excitation laser power is measured by a photodetector (Newport)

just after the polarizers to calibrate the excitation intensity; however, this intensity is not the exact intensity illuminating the sample, as some photons may be loss by reflection on optical components in the microscope or through overfilling of the objective back aperture. An electronic shutter (Uniblitz) is mounted after the polarizers in order to be able to rapidly switch on and off the laser illumination on the sample. The incoming laser beam is directed through the back port of an inverted microscope (Nikon Eclipse TE2000-U), passes a band pass excitation filter (Chroma), and is reflected upwards by a dichroic mirror (Chroma). The beam is then focused through a high numerical aperture water immersion objective (Nikon Plan Fluor, 60x magnification, NA 1.20) into the sample. The sample is constituted of a chamber made of a cover slip mounted on a microscope slide with parafilm bands as spacers, and the chamber is filled with the erythrocyte sample. The fluorescent molecules in the confocal detection volume are excited, and the emitted fluorescence is collected by the same objective. Next, the fluorescence signal is transmitted through the dichroic mirror and an emission filter (Chroma), then it is focused through a motorized pinhole used to remove out-of-focus signal and on the detection window of a photomultiplier tube (Hamamatsu). Another electronic shutter is mounted between the microscope and the pinhole to allow rapidly switching off the signal and to help prevent the photomultiplier tube receiving excessive photon counts. The output signal from the photodetector is sent to a correlator (correlator.com) that computes a trace of the intensity detected with a resolution of 67ms, as well as the corresponding autocorrelation function with a resolution of 8ns. In addition, the microscope has the ability to obtain Differential Interference Contrast (DIC) and wide-field fluorescence images. Image acquisition is done using a frame-transfer CCD camera (Roper Scientific) and the software WinView. The program collects images with either single or multiple frames, and it also includes functions to adjust exposure time for each frame and lag time between frames. All measurements in this project were taken at room temperature.

A signal acquisition and data presentation program was written using LabView (National Instruments) that controls a piezoelectric-driven objective positioner (Physik Instrumente) and the two shutters through an I/O board (National Instruments). It also controls the motorized pinhole. The program was modified from a program written by Daniel Banks that acquires the signal from the correlator and presents the average fluorescence intensity and the autocorrelation function in real time. In addition, the original program aligns the motorized pinhole in three dimensions, to the position that allows receiving the highest photon counts. Additional functions were written for the modified program include a sub-routine that vertically scans the objective position in order to determine membrane position and a sub-routine that records fluorescence intensity traces while allowing to automatically switch on and off the illumination.

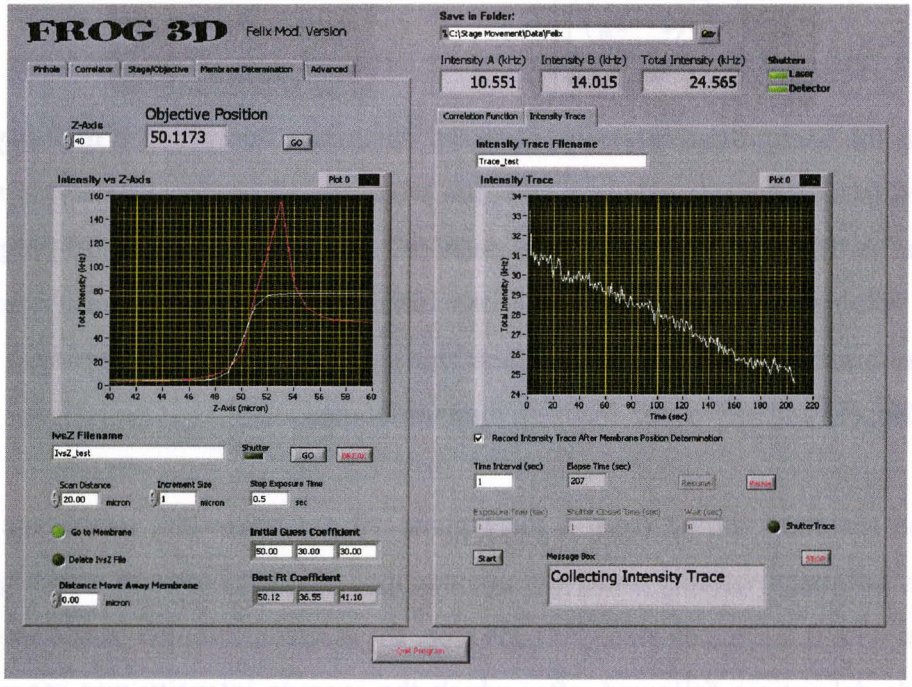

Figure 9. Front panel of the modified experiment control program written using LabView.

2.3 Determination of the erythrocyte membrane position

A method to precisely determine the erythrocyte membrane position in order to place the laser focus exactly on the membrane was developed. This method is based on

the existence of a contrast between the inside and the outside of the cell when fluorescent particles are diffusing in the buffer but not in the cell cytoplasm. By adjusting the height of the objective, the fluorescent particles at different focal plane are excited. The program records the emitted fluorescence and plots the average intensity as a function of vertical position simultaneously. Figure 8 shows an example of the average intensity recorded in the detection volume at various vertical positions with respect to an erythrocyte membrane. If the fluorophores cannot diffuse into the cell cytoplasm, a fraction of the detection volume may contain no fluorophore depending on the membrane position with respect to the detection volume. Assuming the confocal detection volume is a Gaussian revolution ellipsoid (Rigler, Mets et al. 1993), the expression of the vertical one dimensional intensity profile can be written as (Fradin, Abu-Arish et al. 2003):

$$I = I_B + \frac{I_M}{2} \times \left[1 + Erf\left(\frac{\sqrt{2}(z - z_m)}{z_0} \right) \right] \quad (1)$$

where I_B is the background intensity, I_M is the maximum fluorescence intensity that can be detected (which corresponds to a situation when the all confocal detection volume is outside the cell), z_m is the membrane position, and z_0 is the $1/e^2$ half-height of the detection volume. After recording the one dimensional vertical intensity profile, the program automatically determines the membrane position z_m by performing a fit of the data with Eq. (1) and moves the focus on the membrane.

The scanning started from a focal plane 10 μm below the membrane position, which was estimated visually under the microscope. The total upward scanning distance was 20 μm with 0.5 μm step size. At each step, the electronic shutter was opened, then a 0.5 seconds delay time followed, after which the average intensity was recorded for a period of 0.5 seconds. The shutter was closed afterward and the objective was moved to the next step. There was a 0.5 seconds delay time before the shutter opened again. Scans to determine the membrane position were done before and after the local deformation of the membrane to determine the final amplitude and direction of the membrane motion.

2.4 Autocorrelation function analysis

The autocorrelation function of a fluorescent signal, collected using the method of fluorescence correlation spectroscopy (FCS), provides information about the relaxation times of the different processes causing fluorescence fluctuations. For the free diffusion of a single fluorescent species, these fluctuation events represent the diffusion of fluorophores across the detection volume and the relaxation time of the non-fluorescent triplet state. The autocorrelation function for the free diffusion of single fluorescent species is described by (Widengren, Mets et al. 1995):

$$G(t) = \frac{1/N}{\left(1 + t/\tau_d\right)\sqrt{1 + t/S^2\tau_d}}\left(1 + \frac{T\exp(-t/\tau_T)}{1-T}\right) \qquad (2)$$

where N is the average number of fluorophores in the detection volume, τ_d is the fluorophore diffusion time across the detection volume, S is the aspect ratio of the detection volume, τ_T is the relaxation time associated with the non-fluorescent triplet state, and T is the fraction of fluorophores found in the triplet state.

2.5 Calibration

Calibration of the confocal detection volume was performed using fluorescein before each experiment. The autocorrelation functions were obtained from fluorescein (50-80 nM) diffusing freely in the isotonic PBS buffer. Since a single fluorophore species was diffusing in the sample, the obtained autocorrelation functions were fit with the one-component model shown in Eq. (2). All components were calculated by averaging values obtained from four different autocorrelation functions measured in the same sample. The confocal detection volume is assumed to be a 3-D Gaussian which corresponds to an effective ellipsoid having half-width and half-height w_0 and z_0 respectively. Since the diffusion constant for fluorescein is D = 260 $\mu m^2/s$, the radius of

the detection volume, w_0 was determined using the expression (Fradin, Abu-Arish et al. 2003):

$$\tau_d = \frac{w_0^2}{4D} \tag{3}$$

The half-height of the ellipsoid, z_0, was determined from the average aspect ratio ($S = z_0/w_0$). Finally, the effective volume of the confocal detection volume was then calculated using the expression (Fradin, Abu-Arish et al. 2003):

$$V = \pi^{3/2} w_0^2 z_0 \tag{4}$$

The size of the confocal detection volume was changed by adjusting the diameter of the incoming laser beam. Two different radii of the focal volume, 250 nm and 400 nm, could be obtained. Usually, the smaller size of the detection volume was used. In addition, we obtained the autocorrelation functions for the free diffusing fluorescent labeled BSA in the erythrocyte sample. The exact concentration in molar was calculated from the average number of the fluorescently labeled BSA molecules in the detection volume and the known size of the detection volume. This method hence yields a very precise measurement of fluorophore concentration in solution.

2.6 Membrane kinetics experiments

To record the dynamics of the membrane motion, the fluorescence intensity produced by fluorophores diffusing close to the membrane was recorded as a function of time. An example of such a fluorescence intensity trace is shown in Figure 10. The intensity traces obtained on the erythrocyte membrane were described by the expression:

$$I(t) = I_{Max} - (I_{Max} - I_{Min}) \times \exp\left(-t/\tau\right) \tag{5}$$

where I_{Max} is the maximum intensity, I_{Min} is the minimum intensity, and τ is the time constant associated with the local deformation of the membrane. At least nine measurements on different erythrocytes were done and the time constants obtained were

averaged to determine the membrane dynamics under various conditions. The uncertainty was determined by the standard deviation of the measurements.

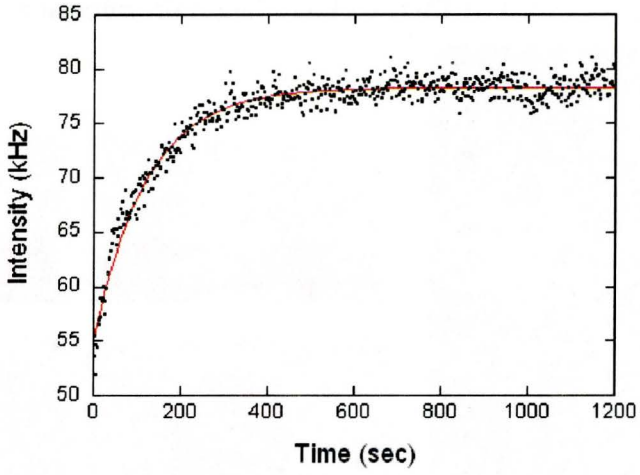

Figure 10. Intensity trace recorded during the erythrocyte membrane local deformation induced by illumination of the erythrocyte membrane with a 20 μW focused laser beam in presence of a 1 μM concentration of fluorescently labeled BSA in the buffer. The red line indicates the best fit to the data using Eq. (5): I_{Max} = 78.3 kHz; I_{Min} = 55.3 kHz; τ = 120 sec.

Chapter 3 Results

3.1 Photodamage induced by focused laser beam illumination

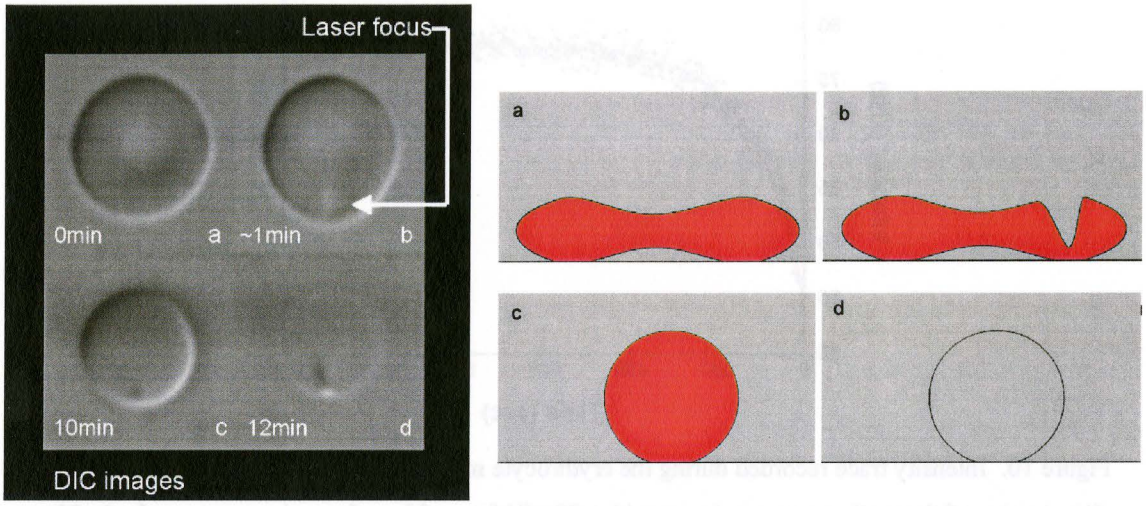

Figure 11. DIC images (left) and schematic representations (right) of RBC photohemolysis at different stages. Photohemolysis was induced by a 150μW focused laser beam with 400 nM of BSA labeled with Alexa Fluor 488 diffusing freely outside the erythrocyte.

The process of hemolysis induced by a focused laser beam illumination can be separated into four stages as shown in Fig. 11. The erythrocyte appears in its normal biconcave disk shape before the laser illumination (Fig. 11a). After about 30 seconds of focused laser illumination on the rim region of the erythrocyte, a local deformation develops on the membrane in the shape of a small imprint at the point of laser illumination (Fig. 11b). The erythrocyte loses its biconcave disk shape gradually with continuous laser illumination and the cell turns to spherical in shape (Fig. 11c). The cell bursts shortly after it has turned into a sphere. If the laser illumination is continued, an aggregate forms at the point of illumination on the erythrocyte ghost membrane (Fig. 11d). The hemolysis time refers to the time taken to burst an erythrocyte. It is measured by starting the clock right after the illumination started and stopping it when the cell burst is observed; for instance, the hemolysis time measured for the cell shown in Fig. 11 was about 12 minutes.

3.2 Control experiments

The influences of various sample conditions on hemolysis time were investigated to determine potential sources of error during the measurements. For instance, I investigated the correlation between the length of time spent by the erythrocytes in vitro and the hemolysis time (Fig. 12). The figure shows that the hemolysis time decreases when the erythrocytes have been outside of the body for several hours under the conditions we kept them in. This suggests that the photohemolytic rate is influenced by the freshness of the erythrocyte sample.

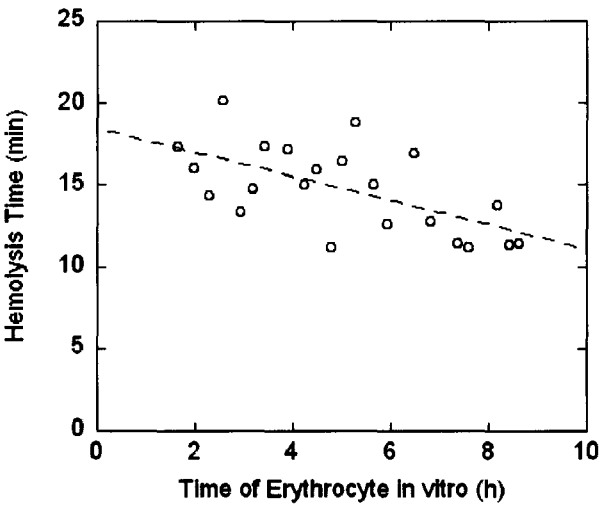

Figure 12. The correlation between the time spent by the erythrocytes in vitro and the hemolysis time. Each data point represents one measurement. Laser input power = 150 μW. Fluorophore concentration ~ 38 nM of BSA labeled with Alexa Fluor 488. The broken line indicates the best fit of the data.

Another control experiment was to investigate the influence of erythrocyte concentration (hematocrit) on the hemolysis time induced by laser illumination. Two hematocrits, 2 % and 0.1 %, were investigated with 150 μW laser input power in conjunction with 38 nM of BSA labeled with Alexa Fluor 488. I found that 2 % and 0.1 % hematocrit gave hemolysis times of 16.4 ± 0.7 min and 17 ± 2 min respectively. Both measurements are in agreement which suggests that the erythrocyte concentration does not affect the rate of hemolysis induced by focused laser beam illumination.

The function of the non-fluorescent labeled BSA is to stabilize the erythrocyte shape. Since BSA is a major component in the buffer, it is important to understand the effect of the BSA concentration in the sample on the hemolysis. Two erythrocyte samples were prepared, one with 1 mg/mL and the other with 10 mg/mL of non-fluorescent labeled BSA. Additionally, both samples contained 38 nM of BSA labeled with Alexa Fluor 488. The samples were then illuminated with a 150 μW focused laser beam. The sample with 1 mg/mL of BSA gave 13 ± 2 min for hemolysis time, and the sample with 10 mg/mL of BSA gave 14 ± 1 min for hemolysis time. The agreement of hemolysis time between the two samples suggests that the rate of photohemolysis is largely independent of the non-fluorescent BSA concentration in the sample.

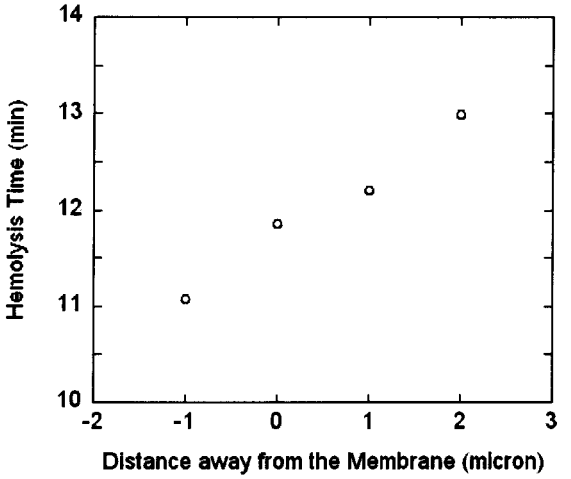

Figure 13. Hemolysis time obtained for various vertical position of the laser focus with respect to the erythrocyte membrane with distance 0 representing the membrane position. Laser input power = 150 μW. Fluorophore concentration = 38 nM of BSA labeled with Alexa Fluor 488.

The counting towards hemolysis time starts right after the automatic membrane position determination. If the intensity profile cannot be fitted by Eq. (2) perfectly, the determined membrane position may be inaccurate. Therefore, it is essential to investigate the effect on hemolysis time of slight vertical mis-positioning of the laser beam with respect to the membrane. The result shown in Fig. 13 suggests that the rate of hemolysis is indeed affected if the laser beam is focused away from the membrane. As a result, the

accuracy of the membrane position determination before the continuous laser illumination is crucial in terms of minimizing the uncertainty on the hemolysis time.

3.3 Intensity trace recorded during photohemolysis

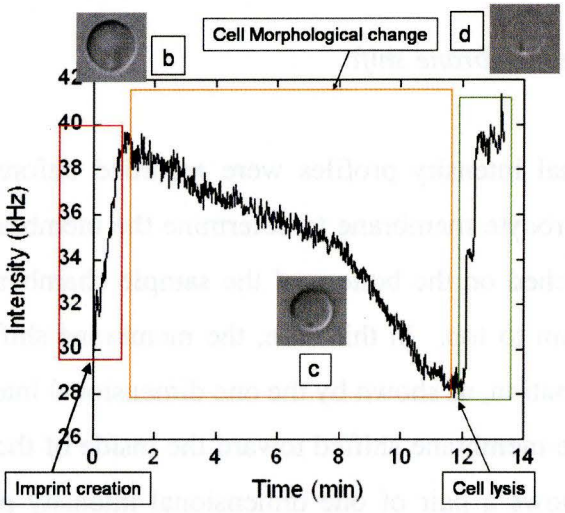

Figure 14. Fluorescence intensity trace recorded during the hemolysis induced by focused laser beam illumination. Laser input power = 150 μW. Fluorophore concentration = 1000 nM of BSA labeled with Alexa Fluor 488.

The measurement of a fluorescence intensity trace is done by focusing the laser beam at the erythrocyte membrane and recording the fluorescence intensity as a function of time while the laser focus is maintained at that fixed position. The intensity trace in Fig. 14 shows that the hemolytic process induced by focused light illumination can be separated into different regions. Each region represents a different response of the erythrocyte during the illumination. The intensity increase in the beginning reflects the imprint creation on the cell membrane because the membrane distortion at the focus allows more fluorophores to enter the detection volume. This is followed by a gradual decrease in intensity which corresponds to a gradual change in cell morphology, from a biconcave disk shape to a spherical shape. Hemolysis occurs at the minimum point. The

sudden increase in intensity indicates that the fluorophore can diffuse across the membrane after the cell has burst.

3.4 Imprint characterization

3.4.1 Direction of the membrane shift

One dimensional intensity profiles were recorded before and after the imprint formation on the erythrocyte membrane to determine the membrane position. When the erythrocytes were attached on the bottom of the sample chamber, the laser illumination direction is from bottom to top. In this case, the membrane shifted to a lower position during the imprint formation, as shown by the one dimensional intensity profiles shown in Fig. 15. Therefore, the membrane shifted toward the inside of the cell at the point of the imprint. Figure 16 shows a pair of one dimensional intensity profiles recorded for an erythrocyte attached to the top glass surface of the sample chamber before and after imprint creation. In this case, the laser beam is focused on the bottom of the cell to create an imprint and the direction of laser illumination is from top to bottom of the cell. The intensity profile indicates that the membrane shifted to a higher vertical position, again the membrane shifted toward the inside of the cell. By determining the membrane position before and after imprint formation using Eq. (2), the local displacements of the membrane at the imprint for both laser illumination directions were determined to be 1.1 ± 0.1 μm (bottom-to-top) and 1.20 ± 0.07 μm (top-to-bottom). Both values are comparable to the thickness of the rim region of an erythrocyte, which is 2.84 μm (Fung, Tsang et al. 1981). The difference in maximum intensity before and after the imprint creation is due to light absorption by hemoglobin when the laser beam travels from bottom to top of the cell. After the imprint formation, the thickness of an erythrocyte at the point of illumination decreases, which reduces light absorption. Therefore, the

maximum fluorescence intensity of the intensity profile recorded after the imprint creation is higher than before the imprint creation.

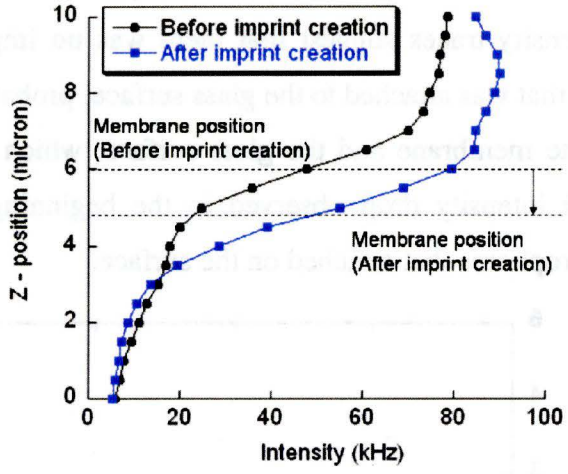

Figure 15. Intensity profiles recorded along a vertical axis of an erythrocyte's rim region when the cell was attached on the bottom glass in the sample chamber. Laser input power = 20 μW. Fluorophore concentration ~ 60 nM of BSA labeled with 488 Alexa Fluor.

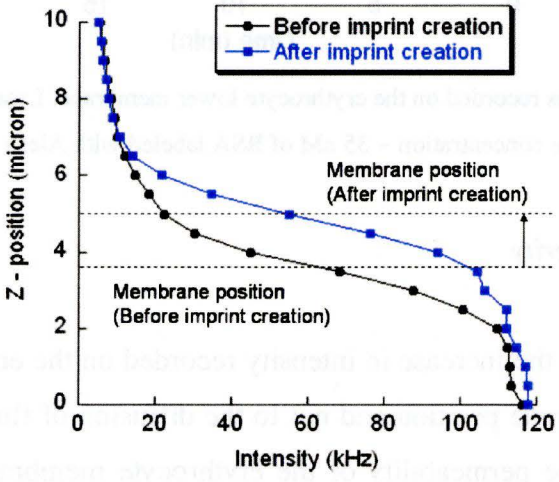

Figure 16. Intensity profile recorded along a vertical axis of an erythrocyte's rim region when the cell was attached on the top glass in the sample chamber. Laser input power = 20 μW. Fluorophore concentration ~ 70 nM of BSA labeled with 488 Alexa Fluor.

Also, the influence of direction of laser illumination on imprint formation was investigated by illuminating the focused laser beam on the erythrocyte membrane in

contact with the glass cover slip when the cell was attached to the bottom glass surface of the sample chamber. Two fluorescence intensity traces were recorded when the laser beam was focused on the bottom membrane, and they are shown in Figure 17. The relatively constant intensity traces suggest that there was no imprint formation on the erythrocyte membrane that was attached to the glass surface, probably due to the adhesion between the erythrocyte membrane and the glass surface, which could prevent imprint formation. The small intensity drop observed in the beginning is likely due to the photobleaching of fluorophores that attached on the surface.

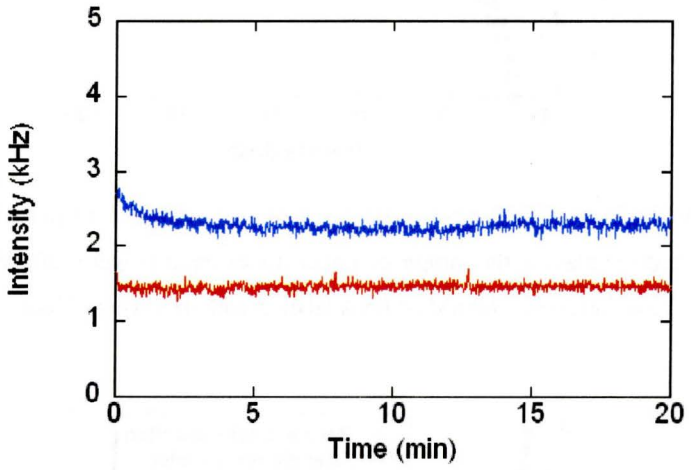

Figure 17. Intensity traces recorded on the erythrocyte lower membrane. Laser input power = 15 μW. Fluorophore concentration ~ 35 nM of BSA labeled with Alexa Fluor 488.

3.4.2 Membrane integrity

To confirm that the increase in intensity recorded on the erythrocyte membrane is due to a shift in membrane position and not to the diffusion of fluorophores into the cell through the imprint, the permeability of the erythrocyte membrane to the fluorophores after imprint creation was investigated. Two kinds of fluorophores were chosen in two separated experiments, fluorescein (332 Da) and BSA labeled with Alexa Fluor 488 (66,000 Da). Both fluorophores are unable to diffuse across the intact erythrocyte membrane. Wide-field fluorescence images were obtained on the erythrocyte samples after the imprint formation on selected erythrocytes. Areas containing no fluorophore

appear dark in color in wide-field fluorescence images. Images in Fig. 18 b) and c) show that fluorescein did not diffuse across the membrane into the erythrocytes for at least one hour after the imprints were created on the erythrocytes. A similar result was obtained from the sample with fluorescently labeled BSA. This shows that no fluorophore with a size larger than 332 Da can diffuse across the membrane into erythrocytes through the imprints and the change in intensity after the imprint formation is proven to be due to a shift of the membrane position at the point of illumination.

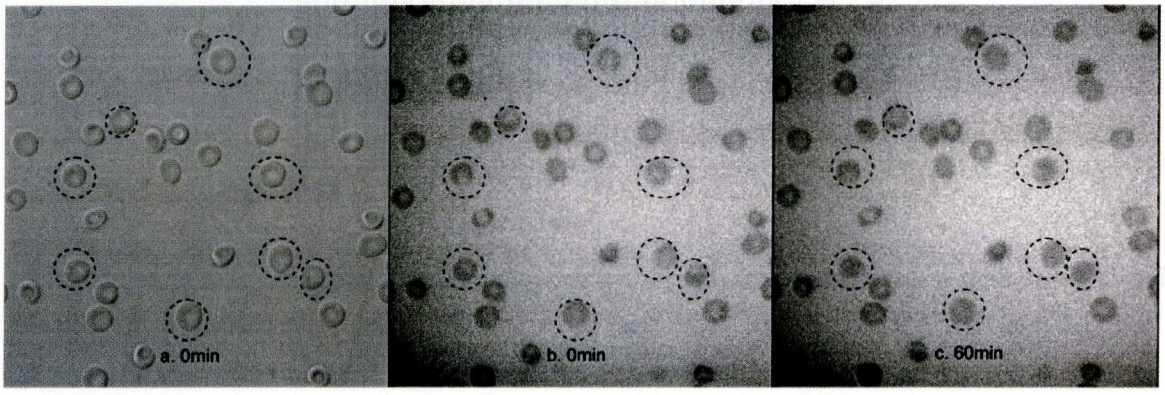

Figure 18. a) DIC image of erythrocytes immediately after creating imprints on all circled erythrocytes. b) Wide-field fluorescence image of the same erythrocytes. c) Wide-field fluorescence image obtained 60 min after image a). Fluorophore concentration ~ 70 nM of fluorescein. Imprint formation was induced by a 20 μW focused laser beam.

3.4.3 Reversibility of imprint formation

The possibility of reversing the imprint formation by stopping the illumination was investigated using a sequence of switching on and off the laser illumination during the recording of fluorescence intensity trace on the erythrocyte. An example of intensity trace recorded with on and off periods of 20s each is shown in Fig. 19. Various combinations of on and off times were investigated and the corresponding imprint formation time constants are tabulated in Table 1. By using the intensity traces obtained for different on and off period combinations, the fluorescence intensities recorded just before and right after the blocking of laser illumination were correlated as illustrated in Fig. 20. A line of slope one is drawn on the graph showing that the data points are not

biased to either side of the line. This result suggests that the membrane position at the imprint does not move when the laser illumination is blocked. The scattering of the data points might be due to the thermal fluctuations of the membrane.

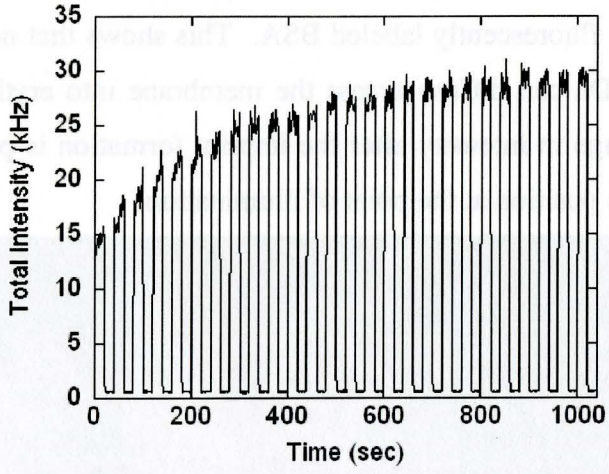

Figure 19. Intensity trace recorded on an erythrocyte membrane with a sequence of switching on and off the laser illumination, t_{on} = 20 s, t_{off} = 20 s. Laser input power = 20 μW. Fluorophore concentration ~ 350 nM of BSA labeled with Alexa Fluor 488.

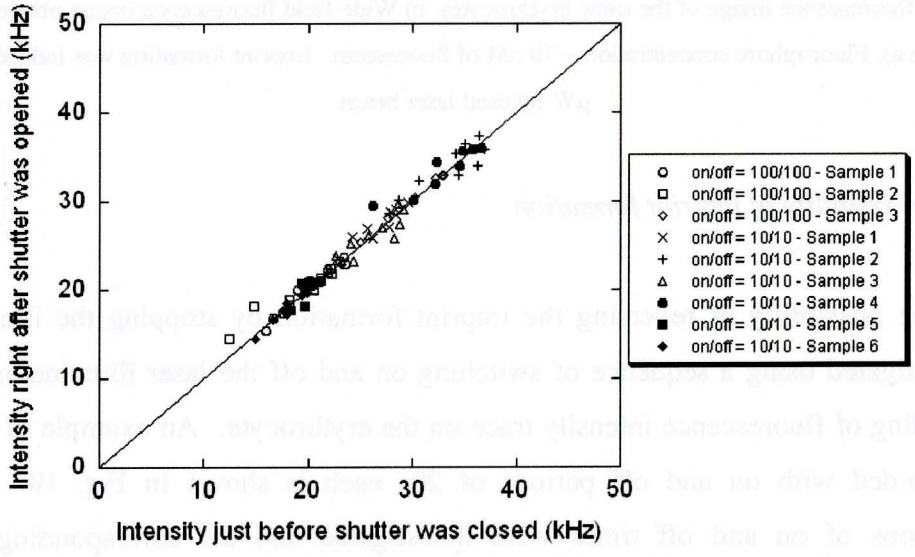

Figure 20. Intensities recorded before and after the off period of the laser illumination from samples with different combinations of on and off period time.

Illumination On Period (s)	Illumination Off Period (s)	Total Time Constant (s)	Time Constant (Off period Removed) (s)	Number of Measurements
10	10	293 ± 194	147 ± 97	6
20	20	296 ± 129	156 ± 60	6
100	100	591 ± 50	305 ± 18	2
5	10	237 ± 62	80 ± 21	9
20	40	319 ± 65	106 ± 22	9
20	80	363 ± 98	73 ± 19	3
5	30	557 ± 321	80 ± 46	3

Table 1 Values of total time constants and time constants with off period removed for different on and off illumination periods.

3.4.4 Investigation of imprint formation on the rim and on the dimple of the erythrocytes

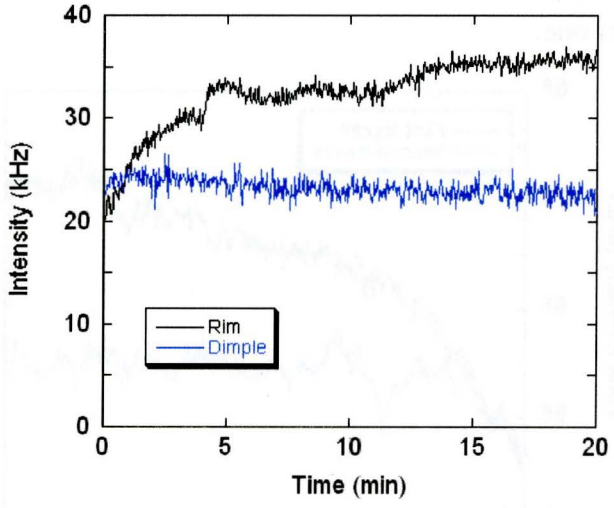

Figure 21. Intensity trace recorded at the rim region and at the dimple for two different erythrocytes. Laser input power = 15 μW. Fluorophore concentration ~ 30 nM of BSA labeled with 488 Alexa Fluor.

Since the thickness of an erythrocyte at the rim and at the dimple are different, the ability of imprint formation induced by laser illumination was investigated at these two regions. The intensity traces recorded on the rim and on the dimple are shown in Fig. 21 together. The result shows that only the laser illumination at the rim creates an imprint on the erythrocyte. Laser illumination at the dimple gave a relatively constant intensity trace;

hence, no imprint was formed at the dimple region of the erythrocyte. This might be due to the small thickness of the dimple region of erythrocytes; therefore, a visible imprint could not form at the dimple region.

3.4.5 Formation of two imprints on the same erythrocyte

The formation of two imprints on the rim region of the same erythrocyte was investigated. An imprint was created at the rim region using laser illumination. Afterward, the focused laser beam was illuminated on the opposite side of the rim region on the same cell to create a second imprint. Two intensity traces representative of these experiments are shown in Fig. 22. The maximum intensity for the second imprint is lower than the first imprint suggesting that the membrane for the second imprint could not move down the same distance as the first imprint; the depth of the second imprint was shallower than the first one.

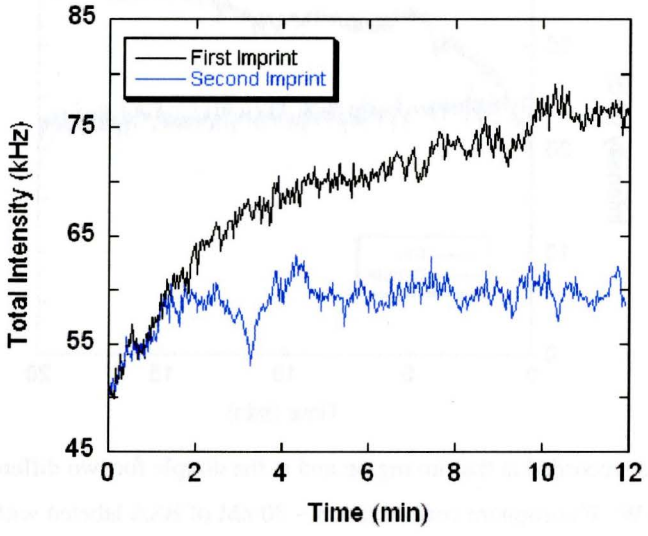

Figure 22. Intensity trace of two imprints formation on the same cell. Laser input power = 20 μW. Fluorophore concentration ~ 48 nM of BSA labeled with 488 Alexa Fluor.

3.5 Kinetics of photohemolysis and imprint formation

3.5.1 Dependence on fluorophore concentration

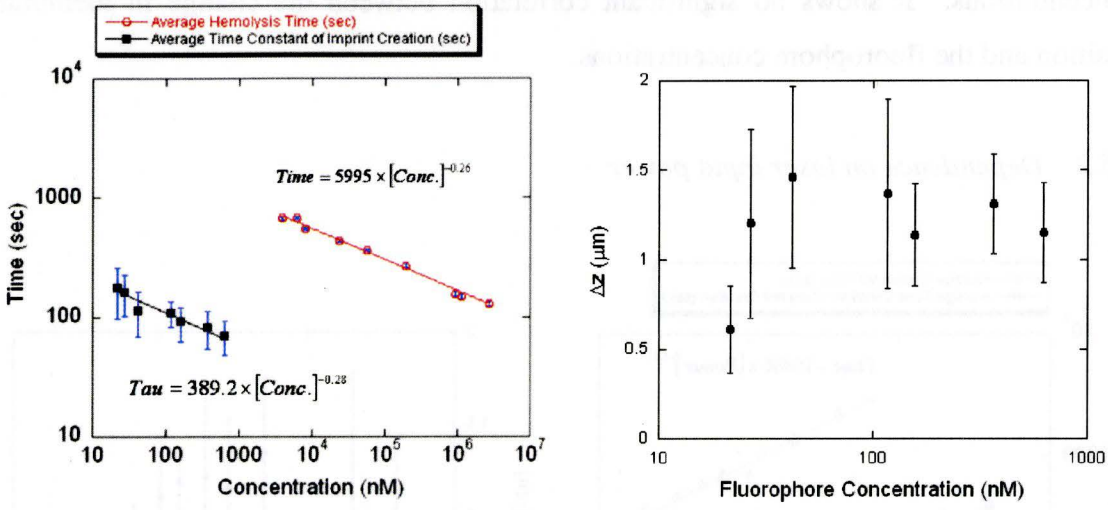

Figure 23. (Left) Average hemolysis time and time constant of imprint formation recorded for various fluorophore concentrations. For photohemolysis, laser input power = 150 μW. For imprint formation, laser input power = 10 μW. (Right) Average change in membrane position during the imprint formation recorded for various fluorophore concentrations.

To determine the effect of fluorophore concentrations on photohemolysis and imprint formation, a fixed laser input power was used. (However, different input powers were used for the study of hemolysis and for the study of imprint formation.) The log-log plot of the hemolysis time and the time constant associated with imprint formation on erythrocyte of samples with various fluorophore concentrations is shown in Fig. 23. In addition, the hemolysis time was determined to be 1120 ± 27 s for sample with no fluorophore using a 150 μW focused laser beam. The results obtained for both processes were fitted with a simple rate equation,

$$R \propto C^{\alpha} I^{\beta} \qquad (6)$$

where R is the reaction rate, C is the external fluorophore concentration, I is the laser input power (fixed in this case), and α and β are the reaction rate orders for the concentration and the intensity respectively. The fits gave the reaction orders of

photohemolysis and imprint formation with respect to fluorophore concentration to be $\alpha = 0.26 \pm 0.02$ and $\alpha = 0.28 \pm 0.04$ respectively. Figure 23 also shows a semi-log plot of the average change in membrane position during imprint formation with various fluorophore concentrations. It shows no significant correlation between the change in membrane position and the fluorophore concentrations.

3.5.2 Dependence on laser input power

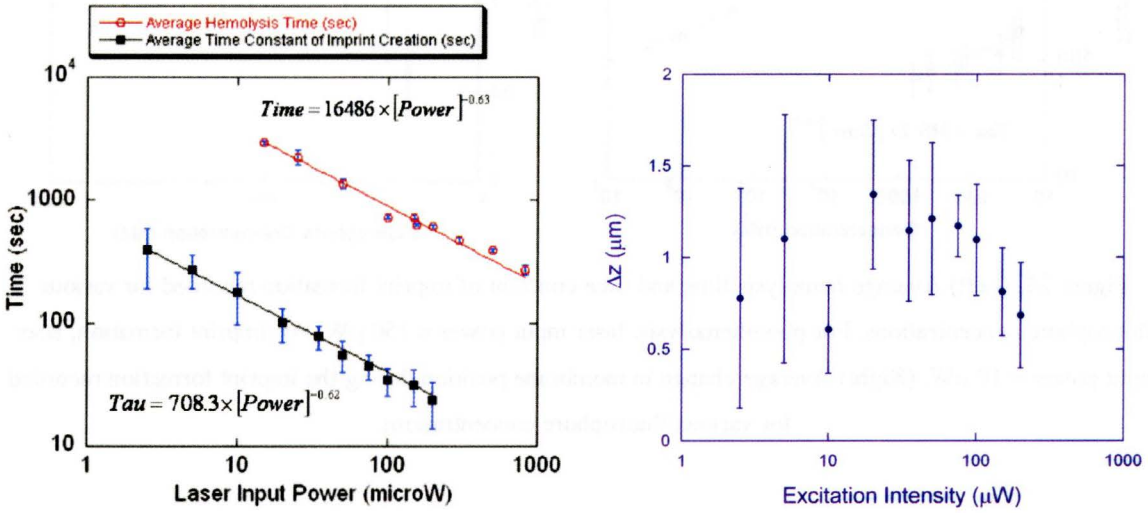

Figure 24. (Left) Average hemolysis time and time constant of imprint formation recorded for various laser input powers. For photohemolysis, fluorophore concentration = 1000nM BSA labeled with Alexa Fluor 488. Each data point was determined averaging five measurements. For imprint formation, fluorophore concentration = 20nM BSA labeled with Alexa 488. Each data point was determined averaging nine measurements. (Right) Average change in membrane position during the imprint formation recorded for various laser input powers.

A fixed fluorophore concentration was used to investigate the effect of varying the laser input power on the rate of photohemolysis and imprint formation. The log-log plots of the hemolysis time and the time constant of imprint formation using various laser input powers is shown in Fig. 24. Once again, each data set was fitted with the simple rate equation, Eq. 6 (keeping C constant). The orders of photohemolysis and imprint formation with respect to laser input power were determined to be $\beta = 0.63 \pm 0.02$ and $\beta =$

0.62 ± 0.04 respectively. The semi-log plot on Fig. 24 shows the average change in membrane position during imprint formation with various laser input power. Again, it suggests that there is no significant correlation between the change in membrane position and the laser input power.

3.5.3 Effect of pH

Furthermore, the effect of pH on the rate of imprint formation was investigated and the result is shown in Fig. 25. A pH range of 6.4 to 7.8 of the buffer was chosen because the erythrocytes can maintain a normal biconcave disk shape within this pH range. Since the uncertainties are large for all data points, the graph shows a relatively constant trend of time constants associated with the imprint formation at different pH. This suggests that the kinetic of imprint formation was independent of (or slightly dependent on) pH between pH = 6.4 to 7.8.

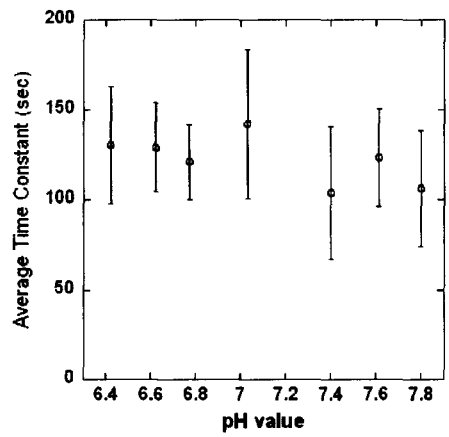

Figure 25. Average time constant of imprint formation recorded for a pH range of 6.4 to 7.8. Laser input power = 20 μW. Fluorophore concentration = 20nM BSA labeled with Alexa Fluor 488.

3.5.4 Overall rate equations

The inverse of the hemolysis time and the time constant have been used to express the reaction rates of the photohemolysis and imprint formation. As a result, the overall reaction rate equation for photohemolysis was described by the expression:

$$R_p = k_1 C^{0.26} I^{0.63}$$

On the other hand, the overall reaction rate equations of imprint formation was described by the expression:

$$R_i = k_2 C^{0.28} I^{0.62}$$

The overall rate orders for photohemolysis and imprint formation were 0.89 ± 0.04 and 0.90 ± 0.06 respectively. The value of overall rate order for both photohemolysis and imprint formation were in agreement; consequently, the photohemolysis and the imprint formation should be highly related processes. The ratio k_1/k_2 was determined to be around 15. Absolute values for k_1 and k_2 can be calculated but meaningless, since I is the laser beam intensity entering the microscope and not at the sample.

3.6 Investigation of the influence of protecting substrates against photodamage

Sodium azide can reduce protein crosslinking and it has been shown to reduce photodamage on the erythrocyte membrane (Lepock, Thompson et al. 1978). Dipyridamole is a band 3 ligand which inhibits anion transport; furthermore, it has been shown to reduce the photodamage on erythrocytes in photodynamic therapy (vanSteveninck, Trannoy et al. 2000). Two erythrocyte samples, one with 10 mM sodium azide and the other with 100 μM dipyridamole, were prepared along with 35 nM of BSA labeled with Alexa Fluor 488 in the sample. The hemolysis times were determined to be 12 ± 1 min for the sample with sodium azide and 4.0 ± 0.6 min for the sample with dipyridamole. By comparison, the control sample with no protecting substrates against photodamage gave 16 ± 1 min for hemolysis time. These results show that not only these two protecting substrates did not reduce photodamage in this case but instead increased the hemolysis rate induced by focused laser beam illumination.

Another protecting substrate, ascorbic acid, was used to investigate the role of oxygen species in the hemolysis induced by focused laser beam illumination (20 μW).

Ascorbic acid (Vitamin C) is an oxygen scavenger which can remove molecular oxygen and quench singlet oxygen. An erythrocyte sample with 5 mM ascorbic acid along with 250 nM of BSA labeled with Alexa Fluor 488 was prepared, and the average hemolysis time was determined to be 20 ± 3 min. In contrast, the average hemolysis time was determined to be 9.0 ± 0.7 min for a control sample without ascorbic acid, a rate of photohemolysis about 2.2 times faster. This result shows that the ascorbic acid reduces hemolysis induced by focused laser beam. Further on, we investigated the effect of the presence of ascorbic acid on the rate of imprint formation (20 μW laser input power). Again, the sample with 5 mM ascorbic acid along with 250 nM of fluorescently labeled BSA was used, and the time constant of imprint formation was determined to be 1.5 ± 0.6 min. On the other hand, the sample without ascorbic acid gave 0.6 ± 0.3 min for the time constant of imprint formation, so the rate of imprint formation is about 2.3 times faster. This suggests that both the rate of photohemolysis and imprint formation do slow down in presence of the oxygen scavenger.

3.7 Focused laser beam illumination on GUVs and HeLa cells

Giant unilamellar vesicles (GUVs) are the simplest cell model and their structure is simpler than erythrocytes. In contrast, HeLa cells are human epithelial cells from cervical cancer tissue and their structures are very different and more complex than erythrocytes. The possibility of imprint formation on GUVs and HeLa cells was investigated to find out whether this process is unique to the erythrocytes. Intensity traces representative of those recorded on GUVs and HeLa cells are shown in Fig. 26 and 27 respectively, where the relative intensity is the ratio of the intensity relative to the maximum average intensity recorded in the sample. Both are relatively constant compared to intensity traces recorded for erythrocytes. One intensity trace recorded on the GUV shows a sudden jump in intensity, and this might be due to a movement of the vesicle since the intensities before and after the jump are relatively constant.

Consequently, the result suggests that imprint formation is a process specific to the cell structure of the erythrocytes. In addition, no lysis of GUVs or HeLa cells was observed for around 30 minutes of laser illumination.

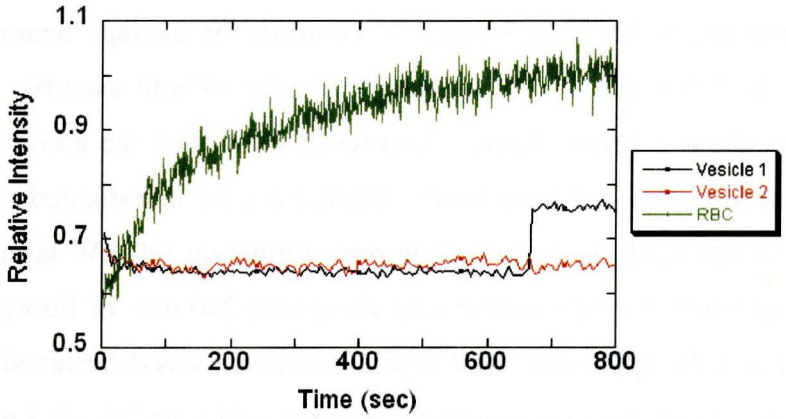

Figure 26. Relative intensity trace recorded on two GUVs (black and red lines) and an erythrocyte (green line). Laser input power = 20 μW. Fluorophore concentration ~ 400 nM of BSA labeled with Alexa Fluor 488.

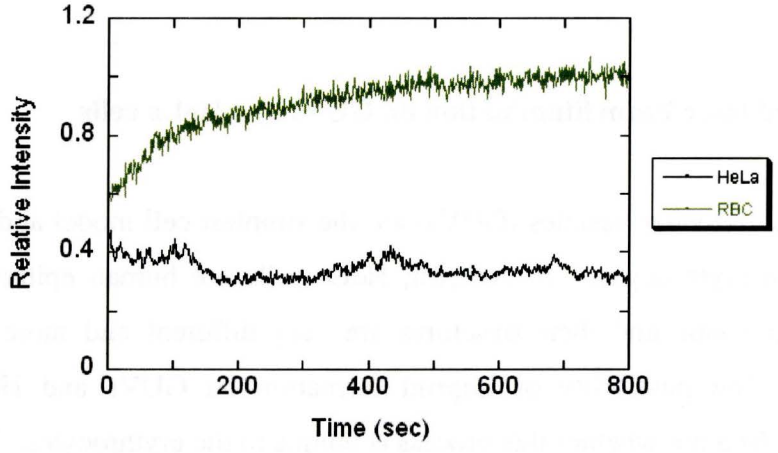

Figure 27. Relative intensity trace recorded on a HeLa cell (black line) and an erythrocyte (green line). Laser input power = 20 μW. Fluorophore concentration ~ 400 nM of BSA labeled with 488 Alexa Fluor.

3.8 Role of erythrocyte components on imprint formation

3.8.1 Imprint formation on erythrocyte ghost

To investigate the role of hemoglobin on imprint formation, resealed erythrocyte ghosts were used since they have the same morphology as the normal erythrocyte except that hemoglobin is absent in ghosts. An erythrocyte ghost with no external fluorophore was illuminated with a focused laser beam on the rim region. Figure 28 shows the DIC images of an erythrocyte ghost before and after the focused laser beam illumination. An imprint was observed on the erythrocyte ghost membrane after the focused laser beam illumination along with a slight cell shape alteration. This suggests that hemoglobin is not a necessary component for imprint formation.

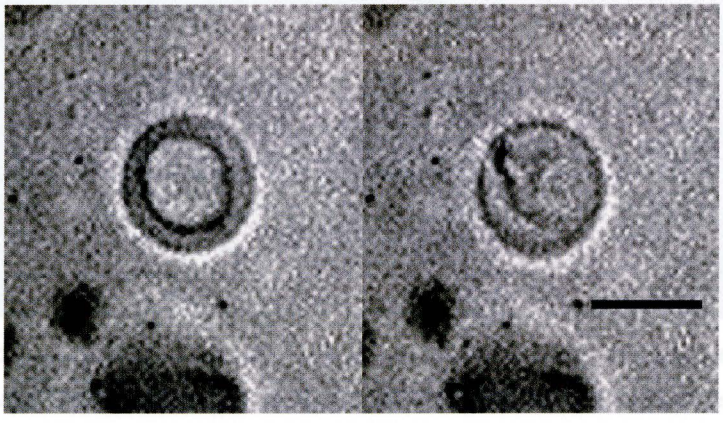

Figure 28. DIC images of a resealed erythrocyte ghost before laser illumination (left) and after laser illumination (right). Laser input power = 100 μW. The sample contained no fluorophore. Scale bar = 5 μm.

3.8.2 Imprint formation on spherical erythrocyte after thermal treatment

Thermal treatment of erythrocytes can remove the function of certain membrane proteins through their thermal denaturation. Spectrin has the lowest denaturation temperature (49°C) of all the erythrocyte membrane related proteins (Lysko, Carlson et al. 1981). To examine the role of spectrin on imprint formation, erythrocytes were heated at 49°C for 10 minutes. This produces spherical erythrocytes, where most of the spectrin is

denatured. Afterward, fluorescein was added into the sample before focused laser beam illumination. The images of spherical erythrocyte before and after the laser illumination are shown on Fig. 29. An imprint was created on the spherical erythrocyte after the laser illumination. Even though this temperature might not be sufficient to denature all the spectrin on the erythrocyte membrane (Lysko, Carlson et al. 1981), this suggests that the imprint could be formed on the spherical erythrocyte with the loss of spectrin. However, the time constant of imprint formation on the temperature treated spherical erythrocytes and normal erythrocytes were determined to be 49 ± 6 s and 16 ± 7 s respectively in the sample with 13 nM of fluorescein and a 50 μW laser intensity. This suggests that the loss of spectrin did slow down the imprint formation and that spectrin does play a role in the imprint formation process.

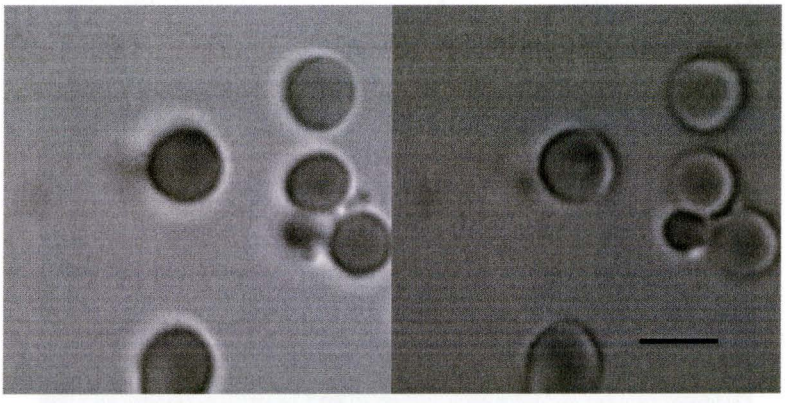

Figure 29. DIC images of a spherical erythrocyte after a 49°C temperature treatment for 10 min. Images were taken before (left) and after (right) a 10 min, focused laser beam illumination. Laser input power = 50 μW. Fluorophore concentration ~ 13 nM of fluorescein. Scale bar = 5 μm.

Chapter 4 Discussions

The progressive hemolysis investigated in this project was induced by focused laser beam illumination on the erythrocyte membrane. The presence of fluorophores in the illuminated sample suggested from the start that the photohemolysis was the result of photosensitized reactions. Prior to hemolysis, an imprint develops on the membrane of the erythrocyte at the point of laser illumination, after which the cell turns to a sphere with a smaller radius than a normal cell. Bloom and Webb observed the same morphological evidence of photodamage in their studies of erythrocyte photodamage in fluorescence photobleaching recovery experiments (Bloom and Webb 1984). In particular, they briefly mentioned the observation of a "pucker" at the point of focused laser beam illumination in the presence of external fluorophores; nevertheless, the cause of the pucker was never studied in detail.

4.1 What is the cause of the imprint?

Three possible effects can be thought of as the cause for imprint formation on the erythrocyte membrane: localized intracellular thermal damage, radiation pressure force, and photosensitized reactions. Bloom and Webb provide a localized intracellular heating calculation at the point of laser illumination on the erythrocyte (Bloom and Webb 1984). In the calculation, they assume that heat is generated at the point of light illumination on the cell surface due to light absorption by hemoglobin, then dissipated into the surrounding medium by heat diffusion and that the temperature reaches a steady state in microseconds. The excitation wavelength is 488 nm in this project, and the molar extinction coefficient for hemoglobin in water at this wavelength is around 24,000 $cm^{-1}M^{-1}$ (Prahl 1998). The calculated temperature shows that the maximum cellular heating of an erythrocyte, given the laser input power used in my experiment (maximum laser input power = 200 μW), should not exceed 3°C. This is too small to create a thermal shock that would damage an erythrocyte since the experiments are carried at room temperature. As

a result, the effect of the localized heating at the point of illumination on the erythrocyte is negligible. As well, radiation pressure force created by the light illumination on the erythrocyte is negligible in this project due to the relatively low laser input power. The typical laser input power necessary to deform erythrocytes using the optical stretcher effect is between 20 mW and 250 mW (Guck, Ananthakrishnan et al. 2000; Guck, Ananthakrishnan et al. 2001). The independence of the direction of laser illumination on membrane shift also suggests that radiation force is not the cause of imprint formation, because in that case, the difference in the light illumination direction should affect the direction of the membrane shift according to the change in momentum of the incident beam. On the other hand, the rate of imprint formation is greatly dependant on the fluorophore concentration, while the creation of radiation force should not be influenced by the fluorophore concentration within the sample. In addition, the irreversible formation of the imprint suggests that the small deformation on the erythrocyte membrane is due to the damage on erythrocyte membrane rather than the radiation force created during the focused laser beam illumination. Therefore, the imprint formation is likely to be the result of photosensitized reactions, but not thermal damage nor radiation pressure. Imprint formation and photohemolysis are also observed in the erythrocyte sample without external fluorophores. Fluorescence microscopy shows that an erythrocyte emit a low fluorescence when the cell is illuminated with a laser beam at both $\lambda = 488$ nm and $\lambda = 543$ nm; therefore, some components of the erythrocyte act as fluorophores at those wavelengths and can induce photosensitization even in the absence of external fluorophore. Additionally, the presence of the oxygen scavenger, ascorbic acid decreases the rate of imprint formation. This suggests that singlet oxygen is created during laser illumination in the sample and that a type II mechanism of the photosensitization is involved in the imprint formation. However, I do not know why other substrates known to protect against photodamage were inefficient at preventing imprint formation. One possibility is that the PBS-RBC buffer used for this study is not suitable for the protecting substrates; for instance, dipyridamole precipitates when dissolved in PBS-RBC buffer. In any case, my experiments show that both the imprint formation and the photohemolysis

induced by focused light illumination are caused by the oxidation of one or several components on the erythrocyte.

4.2 What is the primary target of the photodamage on the erythrocyte?

Once the involvement of photosensitization is established, it becomes crucial to determine the primary target of the photodamage on the erythrocyte. There are a few indications suggesting that band 3 is the primary target causing the imprint formation during focused light illumination. First of all, no imprint forms on the GUVs and HeLa cells; this suggests that the targeted component is found on erythrocytes but not on GUVs nor HeLa cells. Secondly, imprint formation is also observed on erythrocyte ghosts, and this indicates that the target is not in the erythrocyte cytoplasm but instead on the erythrocyte membrane. Thirdly, the dependence of the kinetics of photohemolysis and imprint formation on laser input power and fluorophore concentration are similar, and this indicates that the photohemolysis and imprint formation are highly related processes. Previous studies show that band 3 is the primary target in photohemolysis induced by the non-focused light illumination. Therefore, it is reasonable to conclude that band 3 is also damaged during focused light illumination. A further indication that band 3 degradation is an early process in photodamage came from the work of Josh Ng in our lab, who used immuno-fluorescence probe labeling of band 3 to image erythrocytes. The result shows that band 3 proteins lose the ability to bind the antibodies IgG, which binds to the cytoplasmic domain of band 3, after temporary wide-field illumination (Fig. 30); in fact, this further suggests that it is the cytoplasmic domain of band 3 which is damaged due to the photosensitized reactions. All of the above indications suggest that the degradation of band 3 is involved in both imprint formation and photohemolysis induced by focused light illumination.

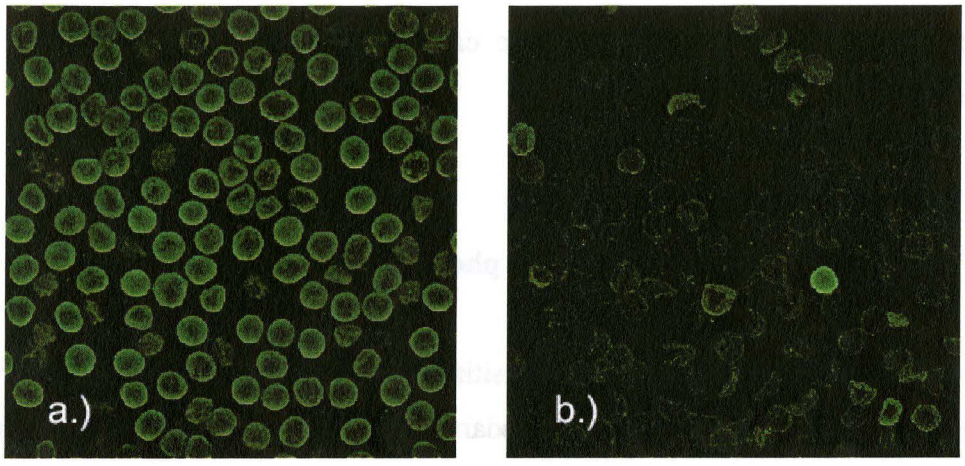

Figure 30. Confocal microscope images of RBCs immunolabeled with an antibody against band 3 a) with 30 min and b) without wide-field illumination before immunolabeling. Photodamaged RBCs have a lower ability to bind band 3 antibodies, which indicates the degradation of band 3 after light illumination. [Photographs taken by Josh Ng]

4.3 Photodamage kinetics of focused and wide-field illumination

Both the rate of photohemolysis and the rate of imprint formation are found to depend on both fluorophore concentration and fluence rate. Furthermore, the order of the dependence on both parameters is exactly the same for the hemolytic and imprint formation process, which depends on the power 0.63 of the fluence and the power 0.26 of the fluorophore concentration. Both rates of photohemolysis and imprint formation are increased 2.2 fold when 5 mM ascorbic acid is added to the sample.

The kinetics of hemolysis induced by wide-field light illumination has been studied intensively. Earlier studies of delayed photohemolysis reported that the hemolytic rate depends on the square of the fluence (Valenzeno and Pooler 1982) and between the power 1.2 and 1.5 of the fluorophore concentration (Valenzeno and Pooler 1982; Valenzeno and Pooler 1982; Pooler 1986). The fluence-squared dependence implies that damages of erythrocytes are formed by the action of two photons. Pooler further suggested that the dimerization of band 3 is the main reason for the involvement of two photons (Pooler 1986). Furthermore, Valenzeno and Pooler suggested that the power

dependence on fluorophore concentration is due to the distribution of sensitizer between the aqueous medium and within the erythrocyte membrane (Valenzeno and Pooler 1982; Valenzeno 1984). However, the dependence of the hemolytic rate on the fluence and the fluorophore concentration that I measured for focused light illumination is different from that observed in the delayed photohemolysis wide-field studies. For delayed photohemolysis experiments, the erythrocyte sample is illuminated with wide-field light for a period of time. Afterward, the sample is incubated in the dark and the percentage of hemolysis is determined through the optical density of the sample after certain time intervals. In this case, the authors tried to understand the long term reaction of photodamaged erythrocytes after a short period of light illumination. My results, on the other hand, were determined with a continuous laser illumination on a small area on a single erythrocyte. In addition, the photon flux in my measurements were a few orders of magnitude higher than the wide-field light illumination experiments. The fluence rates in my experiments were between 500 W/cm^2 and 500 kW/cm^2 compared to a few mW/cm^2 to a few W/cm^2 in the wide-field illumination studies mentioned above. Furthermore, the photodamage in this study is a localized effect compared to the whole cell photodamage in wide-field illumination studies. Considering all the reasons, it seems reasonable that there should be a difference in photosensitized mechanism between the two illumination methods and a difference between the reaction rate orders. More studies will be necessary in order to clarify the dependence of the reaction rates on various conditions; for instance, the effect of using different fluorophore species on the kinetics of imprint formation could give information about the nature of the photodamage mechanism due to the difference in the fluorophore distribution between the cell membrane and the solution.

4.4 Localized vs long range photodamage on the erythrocyte membrane

During focused light illumination of the erythrocyte membrane, only those fluorophores along the beam path are excited and only those band 3 proteins at the point

of laser illumination are damaged. The diffusion distance of singlet oxygen is between 60 nm to 100 nm (Valenzeno 1987), which is a relatively short distance compared to the size of an erythrocyte (~ 8 μm in diameter), so that the singlet oxygen cannot diffuse from one end of the cell to the other end before being deexcited. The relatively short diffusion distance of the singlet oxygen can only create a localized photodamage for immobilized band 3 on the erythrocyte. This localized damage is likely to result in the imprint formation. One important question is: How can this localized damage cause the whole cell to change shape and result in hemolysis? Two-thirds of the band 3 proteins undergo lateral diffusion on the erythrocyte membrane in 37°C (Tomishige, Sako et al. 1998), so damaged band 3 proteins can diffuse in and out of the area of laser illumination. Although the laser illumination is localized, the photodamage of the erythrocyte membrane can be spread to the whole cell through the diffusion of the band 3 proteins and result in hemolysis. The experiment involving the creation of two imprints on the same cell indeed shows the long range effect of the imprint formation. The second imprint always has a shallower depth than the first imprint. Since the lipid membrane of the erythrocyte has a fixed surface area, there is not enough membrane surface area to create a second imprint with the same depth as the first one. In fact, the erythrocyte may provide enough surface area to create a second imprint as deep as the first one by decreasing the depth of the biconcave area of the cell or by decreasing the radius of the cell. However, the creation of the first imprint may change the tension on the cytoskeleton network of the whole cell due to the photodamage of band 3. The result of this increases the rigidity of the cell and makes it harder for the cell harder to change shape.

4.5 Models of erythrocyte shape transformation

Since immobilized band 3 proteins constitute one of the sites connecting the lipid bilayer and the membrane cytoskeleton, it seems logical that they have a functional role

in erythrocyte shape regulation. My experiments indeed indicate that this is the case: oxidation of immobilized band 3 proteins cause a major shape change, the formation of a localized imprint. The simple bilayer coupled theory itself cannot explain the imprint formation because nothing is introduced into either leaflet during the illumination, and most importantly, band 3 is shown to be involved in the imprint formation. The model introduced by Ginsa and Ried on the other hand could explain the erythrocyte morphological change if the photodamage of band 3 was favoring the inward facing of the protein; consequently, localized illumination would promote a cup-shape formation at that point, resulting in an imprint. On other possible explanation for the imprint formation using the area difference elasticity model is that the focused light exposure on the erythrocyte membrane could lead to band 3 protein cross-linking, and band 3 aggregation (a phenomenon which is known to happen when band 3 ages (Turrini, Arese et al. 1991)) Due to the connection between the cytoplasmic domain of band 3 and the spectrin meshwork, band 3 cross-linking or disassociation of band 3 and the cytoskeleton would certainly influence the cytoskeleton shear and stretch modulus at the point of laser illumination. The change in the cytoskeleton shear and stretch elasticities might cause the membrane to adopt the negative curvature observed at the point of illumination, developing an imprint. Another explanation for the imprint formation would be the theoretical model proposed by P. Wong. The oxidation of band 3 might induce the outward facing conformation of band 3 to be favored at the point of laser illumination, which according to the model would promote the unfolding of the spectrin at that point. This action would relax the cytoskeleton network at the point of the laser illumination, leading the membrane to develop an imprint.

4.6 Involvement of spectrin in imprint formation

Thermal denaturation of spectrin on erythrocyte membranes at 49°C causes the cell to turn to a spherical shape. However, differential scanning calorimetry (DSC) experiments shows a broad transition temperature of denaturing spectrin, indicating that

not all the spectrin is denatured at this temperature (Appell and Low 1982; Lepock, Frey et al. 1989), and the exact amount of spectrin which is denatured after heating an erythrocyte sample at 49°C for 10 minutes is unknown. This means that the slower rate for imprint formation detected in these conditions could be due to different effects. Nevertheless, it shows that spectrin plays a role on imprint formation. Furthermore, it reinforces the idea that the functional role of band 3 lies in its connection with the cell cytoskeleton. According to all the results of this project, the shape transformation model proposed by P. Wong appears to be the most likely model in order to explain erythrocyte shape changes; however, my results do not support the mechanism he proposed directly; my results support only the components of his model, namely the involvement of band 3 through its connection to spectrin. More experiments are needed to determine how the kinetics of imprint formation changes after the erythrocyte samples are treated at different temperatures. Band 3 has the highest denaturation temperature compared to the other erythrocyte membrane proteins, which are 62°C for the cytoplasmic domain and 68°C for the transmembrane domain (Appell and Low 1982). Therefore, it is possible to denature erythrocyte membrane proteins except band 3 using thermal treatment. This method will allow to verify whether imprint formation is possible with band 3 proteins alone, in the absence of spectrin. The result of a preliminary DSC experiment for erythrocyte membranes is shown in Fig. 31. One broad thermal transition peak is observed instead of the three distinct peaks usually recorded for erythrocyte ghosts, probably due to the aggregation of the ghosts after the few intense centrifugations performed to remove hemoglobin from the solution. Nevertheless, the data can be fitted with the summation of three Gaussian function with distinct transition temperatures 50.5°C, 59.6°C, and 65.9°C, and they are closed to the published values (Lepock, Frey et al. 1989). This shows that the erythrocyte ghosts stored in the buffer I used can produce the same denaturation temperatures as the published values.

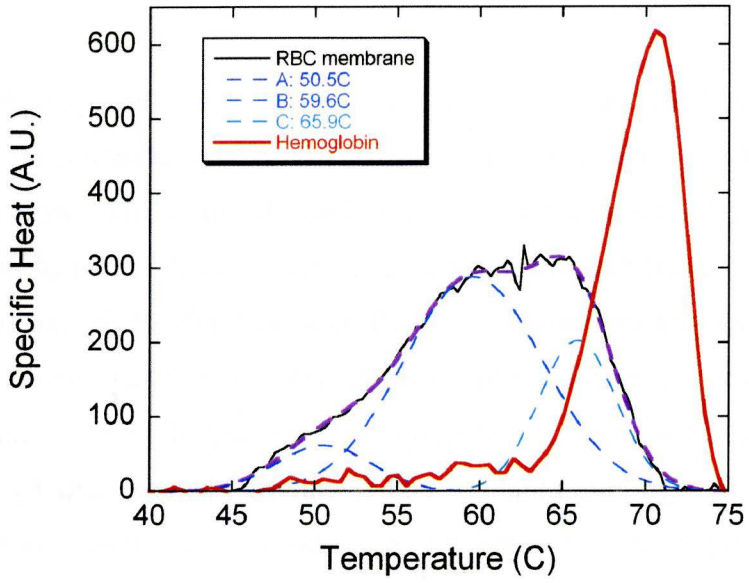

Figure 31. DSC scans (40-75°C) of human erythrocyte ghost with (red line) and without (black line) hemoglobin. Three Gaussian functions with three different thermal transition temperatures are shown and the summation of the three functions produces the curve fit of the DCS scan of the erythrocyte ghost (purple broken line).

Chapter 5 Conclusions

The main tasks undertaken in this project were the characteristization and determination of the formation mechanism of the imprint observed on the erythrocyte membrane when illuminated with focused laser beam in the presence of external fluorophores. I showed that the erythrocyte membrane at the point of the imprint shifts roughly 1.2 μm toward the inside of the cell, independently of the direction of the light illumination. Also, the imprint formation on the erythrocyte is an irreversible equilibrium process. The imprint formation is the first observable step of the photoinduced hemolysis caused by focused light illumination, and it can be characterized by an exponential equation, which represents a formation rate. I showed that the imprint formation is the result of band 3 oxidation. It confirms that band 3 plays a pivotal role in the preservation of the erythrocyte morphology and in inducing rapid shape changes.

This project also introduced a new strategy to study the specific role of erythrocyte membrane proteins in the mechanism of the erythrocyte shape changes using thermal denaturation of proteins. My results showed that the rate of imprint formation becomes slower after most of the spectrin on the erythrocyte membrane being thermally denatured, which it suggests spectrin plays a role in imprint formation. Further experiments are needed in order to determine the exact influence of different proteins on imprint.

To conclude this project, my study may provide several clues to understand the erythrocyte. Studying the localized photodamage of erythrocyte may provide insight on the cell components that involved in the overall photohemolysis process. Also, it may provide insight on models for erythrocyte shape changes. This project further suggests that experimental techniques involving fluorescence and focused laser beams such as FRAP, FCS, and confocal microscopy, should be used cautiously for cell membrane studies, especially for the study of the erythrocyte membrane.

References

Alberts, B., D. Bray, et al. (1994). Molecular Biology of the Cell. New York, Garland Publishing.

Alloisio, N., N. Dalla Venezia, et al. (1993). "Evidence that red blood cell protein p55 may participate in the skeleton-membrane linkage that involves protein 4.1 and glycophorin C." Blood **82**(4): 1323-7.

Anderson, R. A. and R. E. Lovrien (1984). "Glycophorin Is Linked by Band-4.1 Protein to the Human-Erythrocyte Membrane Skeleton." Nature **307**(5952): 655-658.

Appell, K. C. and P. S. Low (1982). "Evaluation of Structural Interdependence of Membrane-Spanning and Cytoplasmic Domains of Band-3." Biochemistry **21**(9): 2151-2157.

Ashkin, A. (1997). "Optical trapping and manipulation of neutral particles using lasers." Proceedings of the National Academy of Sciences of the United States of America **94**(10): 4853-4860.

Ashkin, A. (2000). "History of optical trapping and manipulation of small-neutral particle, atoms, and molecules." Ieee Journal of Selected Topics in Quantum Electronics **6**(6): 841-856.

Ashkin, A. and J. M. Dziedzic (1987). "Optical Trapping and Manipulation of Viruses and Bacteria." Science **235**(4795): 1517-1520.

Ashkin, A., J. M. Dziedzic, et al. (1987). "Optical Trapping and Manipulation of Single Cells Using Infrared-Laser Beams." Nature **330**(6150): 769-771.

Bennett, V. and A. J. Baines (2001). "Spectrin and ankyrin-based pathways: Metazoan inventions for integrating cells into tissues." Physiological Reviews **81**(3): 1353-1392.

Bennett, V. and P. J. Stenbuck (1979). "Membrane Attachment Protein for Spectrin Is Associated with Band-3 in Human-Erythrocyte Membranes." Nature **280**(5722): 468-473.

Bertles, J. F. and P. F. Milner (1968). "Irreversibly sickled erythrocytes: a consequence of the heterogeneous distribution of hemoglobin types in sickle-cell anemia." J Clin Invest **47**(8): 1731-41.

Bessis, M. (1973). Red cell shapes. An illustrated classification and its rationale. Red cell shape: physiology, pathology, ultrastructure. M. Bessis, Weed, R.I., Leblond, P.F. New York, Springer-Verlag: 180.

Beth, A. H., K. Balasubramanian, et al. (1981). "Structural and Motional Changes in Glyceraldehyde-3-Phosphate Dehydrogenase Upon Binding to the Band-3 Protein of the Erythrocyte-Membrane Examined with [N-15,H-2]Maleimide Spin Label and Electron-Paramagnetic Resonance." Proceedings of the National Academy of Sciences of the United States of America-Biological Sciences **78**(8): 4955-4959.

Bloom, J. and W. Webb (1984). "Photodamage to intact erythrocyte membranes at high laser intensities: methods of assay and suppression." J. Histochem. Cytochem. **32**(6): 608-616.

Boal, D. (2002). Mechanics of the Cell, Cambridge University Press.

Byers, T. J. and D. Branton (1985). "Visualization of the Protein Associations in the Erythrocyte-Membrane Skeleton." Proceedings of the National Academy of Sciences of the United States of America **82**(18): 6153-6157.

Cadet, J., M. Berger, et al. (1986). "Photosensitized Reactions of Nucleic-Acids." Biochimie **68**(6): 813-834.

Cassoly, R. (1982). "Interaction of Hemoglobin with the Red-Blood-Cell Membrane - a Saturation Transfer Electron-Paramagnetic Resonance Study." Biochimica Et Biophysica Acta **689**(2): 203-209.

Christiansson, A., F. A. Kuypers, et al. (1985). "Lipid Molecular Shape Affects Erythrocyte Morphology - a Study Involving Replacement of Native Phosphatidylcholine with Different Species Followed by Treatment of Cells with Sphingomyelinase-C or Phospholipase-A2." Journal of Cell Biology **101**(4): 1455-1462.

Discher, D. E. and P. Carl (2001). "New insights into red cell network structure, elasticity, and spectrin unfolding--a current review." Cell Mol Biol Lett **6**(3): 593-606.

Fairbanks, G., T. L. Steck, et al. (1971). "Electrophoretic analysis of the major polypeptides of the human erythrocyte membrane." Biochemistry **10**(13): 2606-17.

Fischer, F., M. Aulmann, et al. (1998). "Blood cell damage after in vitro irradiation of fresh whole blood with 630 nm laser light." Blood Cells Molecules and Diseases **24**(18): 385-395.

Fradin, C., A. Abu-Arish, et al. (2003). "Fluorescence Correlation Spectroscopy Close to a Fluctuating Membrane." Biophys. J. **84**(3): 2005-2020.

Fung, Y. C., W. C. O. Tsang, et al. (1981). "High-Resolution Data on the Geometry of Red-Blood-Cells." Biorheology **18**(3-6): 369-385.

Gardner, K. and V. Bennett (1987). "Modulation of Spectrin Actin Assembly by Erythrocyte Adducin." Nature **328**(6128): 359-362.

Gedde, M. M., E. Y. Yang, et al. (1995). "Shape Response of Human Erythrocytes to Altered Cell Ph." Blood **86**(4): 1595-1599.

Gedde, M. M., E. Y. Yang, et al. (1999). "Resolution of the paradox of red cell shape changes in low and high pH." Biochimica Et Biophysica Acta-Biomembranes **1417**(2): 246-253.

Gimsa, J. and C. Ried (1995). "Do Band-3 Protein Conformational-Changes Mediate Shape Changes of Human Erythrocytes." Molecular Membrane Biology **12**(3): 247-254.

Guck, J., R. Ananthakrishnan, et al. (2001). "The optical stretcher: A novel laser tool to micromanipulate cells." Biophysical Journal **81**(2): 767-784.

Guck, J., R. Ananthakrishnan, et al. (2000). "Optical deformability of soft biological dielectrics." Physical Review Letters **84**(23): 5451-5454.

Henon, S., G. Lenormand, et al. (1999). "A new determination of the shear modulus of the human erythrocyte membrane using optical tweezers." Biophysical Journal **76**(2): 1145-1151.

Hopper, C. (2000). "Photodynamic therapy: a clinical reality in the treatment of cancer." Lancet Oncol **1**: 212-9.

Iglic, A. (1997). "A possible mechanism determining the stability of spiculated red blood cells." Journal of Biomechanics **30**(1): 35-40.

Iglic, A., V. Kralj-Iglic, et al. (1998). "Amphiphile induced echinocyte-spheroechinocyte transformation of red blood cell shape." European Biophysics Journal with Biophysics Letters **27**(4): 335-339.

Kay, M. M. (2004). "Band 3 and its alterations in health and disease." Cellular and Molecular Biology **50**(2): 117-138.

Kay, M. M. B. (1984). "Localization of Senescent Cell Antigen on Band-3." Proceedings of the National Academy of Sciences of the United States of America-Biological Sciences **81**(18): 5753-5757.

Knauf, P. A., P. K. Gasbjerg, et al. (1996). "The asymmetry of chloride transport at 38 degrees C in human red blood cell membranes." Journal of General Physiology **108**(6): 577-589.

Korsgren, C. and C. M. Cohen (1986). "Purification and properties of human erythrocyte band 4.2. Association with the cytoplasmic domain of band 3." J Biol Chem **261**(12): 5536-43.

Lange, Y. and J. M. Slayton (1982). "Interaction of Cholesterol and Lysophosphatidylcholine in Determining Red-Cell Shape." Journal of Lipid Research **23**(8): 1121-1127.

Lee, J. C. M., D. T. Wong, et al. (1999). "Direct measures of large, anisotropic strains in deformation of the erythrocyte cytoskeleton." Biophysical Journal **77**(2): 853-864.

Lenormand, G., S. Henon, et al. (2001). "Direct measurement of the area expansion and shear moduli of the human red blood cell membrane skeleton." Biophysical Journal **81**(1): 43-56.

Lepke, S., H. Fasold, et al. (1976). "Study of Relationship between Inhibition of Anion-Exchange and Binding to Red Blood-Cell Membrane of 4,4'-Diisothiocyano Stilbene-2,2'-Disulfonic Acid (Dids) and Its Dihydro Derivative (H2dids)." Journal of Membrane Biology **29**(1-2): 147-177.

Lepke, S. and H. Passow (1976). "Effects of Incorporated Trypsin on Anion-Exchange and Membrane Proteins in Human Red Blood-Cell Ghosts." Biochimica Et Biophysica Acta **455**(2): 353-370.

Lepock, J. R., H. E. Frey, et al. (1989). "Relationship of hyperthermia-induced hemolysis of human erythrocytes to the thermal denaturation of membrane proteins." Biochim Biophys Acta **980**(2): 191-201.

Lepock, J. R., J. E. Thompson, et al. (1978). "Photoinduced crosslinking of membrane proteins by fluorescein isothiocyanate." Biochemical And Biophysical Research Communications **85**(1): 344-350.

Lim, H. W. G., M. Wortis, et al. (2002). "Stomatocyte-discocyte-echinocyte sequence of the human red blood cell: Evidence for the bilayer-couple hypothesis from membrane mechanics." Proceedings of the National Academy of Sciences of the United States of America **99**(26): 16766-16769.

Liu, S. C. and L. H. Derick (1992). "Molecular Anatomy of the Red-Blood-Cell Membrane Skeleton - Structure-Function-Relationships." Seminars in Hematology **29**(4): 231-243.

Liu, S. C. and J. Palek (1980). "Spectrin Tetramer-Dimer Equilibrium and the Stability of Erythrocyte-Membrane Skeletons." Nature **285**(5766): 586-588.

Low, P. S. (1986). "Structure and Function of the Cytoplasmic Domain of Band-3 - Center of Erythrocyte-Membrane Peripheral Protein Interactions." Biochimica Et Biophysica Acta **864**(2): 145-167.

Lysko, K. A., R. Carlson, et al. (1981). "Protein Involvement in Structural Transitions of Erythrocyte-Ghosts - Use of Thermal Gel Analysis to Detect Protein Aggregation." Biochemistry **20**(19): 5570-5576.

Makropoulou, M., A. Serafetinides, et al. (1995). "The Interaction of He-Ne-Laser Radiation with the Erythrocyte-Membrane." Bioelectrochemistry and Bioenergetics **38**(2): 427-430.

Mukhopadhyay, R., H. W. G. Lim, et al. (2002). "Echinocyte shapes: bending, stretching, and shear determine spicule shape and spacing." Biophys J **82**(4): 1756-72.

Nakao, M. (2002). "New insights into regulation of erythrocyte shape." Curr Opin Hematol **9**(2): 127-32.

Nakao, M., T. Nakao, et al. (1961). "Adenosine triphosphate and shape of erythrocytes." J Biochem (Tokyo) **49**: 487-92.

Ohanian, V., L. C. Wolfe, et al. (1984). "Analysis of the Ternary Interaction of the Red-Cell Membrane Skeletal Protein-Spectrin, Protein-Actin, and Protein 4.1." Biochemistry **23**(19): 4416-4420.

Passow, H. (1986). "Molecular aspects of band 3 protein-mediated anion transport across the red blood cell membrane." Rev Physiol Biochem Pharmacol **103**: 61-203.

Pooler, J. P. (1986). "A new hypothesis for the target in photohemolysis: dimers of the band 3 protein." Photochem Photobiol **43**(3): 263-6.

Pooler, J. P. and A. W. Girotti (1986). "Photohemolysis of human erythrocytes labeled in band 3 with eosin-isothiocyanate." Photochem Photobiol **44**(4): 495-9.

Prahl, S. (1998). Tabulated Molar Extinction Coefficient for Hemoglobin in Water. **2003**. http://omlc.ogi.edu/spectra/hemoglobin/summary.html

Rigler, R., U. Mets, et al. (1993). "Fluorescence correlation spectroscopy with high count rate and low background: analysis of translational diffusion." European Biophysics Journal **22**: 169-175.

Sahr, K. E., P. Laurila, et al. (1990). "The Complete Cdna and Polypeptide Sequences of Human Erythroid Alpha-Spectrin." Journal of Biological Chemistry **265**(8): 4434-4443.

Sato, Y., S. Kamo, et al. (1995). "Mechanism of free radical-induced hemolysis of human erythrocytes: hemolysis by water-soluble radical initiator." Biochemistry **34**(28): 8940-9.

Scheffer, L., A. Bitler, et al. (2001). "Atomic force pulling: probing the local elasticity of the cell membrane." European Biophysics Journal with Biophysics Letters **30**(2): 83-90.

Sheetz, M. P. and D. E. Koppel (1979). "Membrane damage caused by irradiation of fluorescent concanavalin A." Proc Natl Acad Sci U S A **76**(7): 3314-7.

Sheetz, M. P., R. G. Painter, et al. (1976). "Biological-Membranes as Bilayer Couples .3. Compensatory Shape Changes Induced in Membranes." Journal of Cell Biology **70**(1): 193-203.

Sheetz, M. P. and S. J. Singer (1974). "Biological membranes as bilayer couples. A molecular mechanism of drug-erythrocyte interactions." Proc Natl Acad Sci U S A **71**(11): 4457-61.

Shotton, D. M., B. E. Burke, et al. (1979). "Molecular-Structure of Human-Erythrocyte Spectrin - Biophysical and Electron-Microscopic Studies." Journal of Molecular Biology **131**(2): 303-329.

Spikes, J. D. (1989). Photosensitization. The Science of photobiology. K. C. Smith. New York, Plenum Publishing Corporation: 79-110.

Tomishige, M., Y. Sako, et al. (1998). "Regulation mechanism of the lateral diffusion of band 3 in erythrocyte membranes by the membrane skeleton." Journal of Cell Biology **142**(4): 989-1000.

Trannoy, L. L., A. Brand, et al. (2002). "Relation between K+ leakage and damage to band 3 in photodynamically treated red cells." Photochem Photobiol **75**(2): 167-71.

Turrini, F., P. Arese, et al. (1991). "Clustering of Integral Membrane-Proteins of the Human Erythrocyte-Membrane Stimulates Autologous Igg Binding, Complement Deposition, and Phagocytosis." Journal of Biological Chemistry **266**(35): 23611-23617.

Tuvia, S., S. Levin, et al. (1998). "Mechanical fluctuations of the membrane-skeleton are dependent on F-actin ATPase in human erythrocytes." J Cell Biol **141**(7): 1551-61.

Tyler, J. M., W. R. Hargreaves, et al. (1979). "Purification of 2 Spectrin-Binding Proteins - Biochemical and Electron-Microscopic Evidence for Site-Specific Reassociation between Spectrin and Bands 2.1 and 4.1." Proceedings of the National Academy of Sciences of the United States of America **76**(10): 5192-5196.

Ungewickell, E., P. M. Bennett, et al. (1979). "Invitro Formation of a Complex between Cytoskeletal Proteins of the Human-Erythrocyte." Nature **280**(5725): 811-814.

Valenzeno, D. P. (1984). "Photohemolytic lesions: stoichiometry of creation by phloxine B." Photochem Photobiol **40**(6): 681-8.

Valenzeno, D. P. (1987). "Photomodification of Biological-Membranes with Emphasis on Singlet Oxygen Mechanisms." Photochemistry and Photobiology **46**(1): 147-160.

Valenzeno, D. P. and J. P. Pooler (1982). "Cell-Membrane Photo-Modification - Relative Effectiveness of Halogenated Fluoresceins for Photo-Hemolysis." Photochemistry and Photobiology **35**(3): 343-350.

Valenzeno, D. P. and J. P. Pooler (1982). "The Concentration and Fluence Dependence of Delayed Photo-Hemolysis." Photochemistry and Photobiology **35**(3): 427-429.

vanSteveninck, J., L. L. Trannoy, et al. (2000). "Selective protection of RBCs against photodynamic damage by the band 3 ligand dipyridamole." Transfusion **40**(11): 1330-1336.

Voet, D., J. G. Voet, et al. (1999). Fundamentals of Biochemistry. New York, John Wiley & Sons, Inc.

Wang, D. N. (1994). "Band-3 Protein - Structure, Flexibility and Function." Febs Letters **346**(1): 26-31.

Widengren, J., U. Mets, et al. (1995). "Fluorescence Correlation Spectroscopy of Triplet States in Solution: A Theoretical and Experimental Study." Journal of Physical Chemistry **99**: 13368-13379.

Winkelmann, J. C., J. G. Chang, et al. (1990). "Full-Length Sequence of the Cdna for Human Erythroid Beta-Spectrin." Journal of Biological Chemistry **265**(20): 11827-11832.

Wong, P. (1994). "Mechanism of control of erythrocyte shape: a possible relationship to band 3." J Theor Biol **171**(2): 197-205.

Wong, P. (1999). "A basis of echinocytosis and stomatocytosis in the disc-sphere transformations of the erythrocyte." Journal of Theoretical Biology **196**(3): 343-361.